Meissner Levitating Micro Particle

Uitenbroek, Dennis

Meissner Levitating Micro Particle

Thesis

submitted in partial fulfillment of the
requirements for the degree of

Master of Science
in
Physics

Author :	Dennis Uitenbroek BSc
Student ID :	s1697552
Supervisor :	Prof. dr. ir. Tjerk Oosterkamp
	Tim Fuchs MSc
2nd corrector :	Dr. Wolfgang Löffler

Leiden, The Netherlands, June 27, 2022

Meissner Levitating Micro Particle

Dennis Uitenbroek BSc

Huygens-Kamerlingh Onnes Laboratory, Leiden University
P.O. Box 9500, 2300 RA Leiden, The Netherlands

June 27, 2022

Abstract

In between quantum mechanics (QM) and general relativity (GR) there is a regime which holds an upper bound for QM and a lower bound for GR. This thesis focusses on the lower bound of GR in the Newtonian limit.
This thesis describes how gravitational interaction between two masses, a block of 2.4 kg and a magnet of 1.5 mg separated by several decimeters can be measured. This method could be extrapolated to detect gravitational interaction between masses in the order of milligrams. This enables a method to investigate the regime between quantum mechanics and general relativity.
For this experiment a magnet is used levitating inside a superconducting trap. A SQUID is used to measure the oscillation of the levitating magnet. The vertical mode, levitation height, vertical eigenfrequency and vertical rotational eigenfrequency are theoretically predicted. The energy coupling and the method to convert the SQUID signal to a distance are described. A simulation is performed to predict the expected amplitude and phase of the gravitational interaction between the levitating magnet and the larger masses. A calculation shows that the difference in gravitational interaction between the levitating magnet and the moon due to the rotation of the moon is in the order of the oscillation amplitude of the magnet.
As the magnet is excited by sending a flux, a damping time of 5823 s is measured and a Q factor of 960×10^3 is calculated. The energy coupling is determined at 1.40×10^{-11}. The mechanical vibration isolation is characterised by calculating the mechanical damping in the system. This is done using an actuator (111 dB) and using the masswheel as a source of vibrations (92 dB). The difference could be explained by gravitational interaction or by different couplings of mechanical vibrations.
The gravitational amplitude and phase is plotted in the simulated data. It is unknown to which mode the frequency corresponds. The amplitude and phase do not agree on which mode the frequency corresponds to. The amplitude suggests it would be an x- or z-mode with an x- or y-displacement while the phase suggests it would be either the y-mode with an x-displacement or the x- or z-mode with a y-displacement.
Several improvements are proposed to eventually enable a new approach to investigate the regime in between quantum mechanics and general relativity.

Contents

Chapter 1

Introduction

1.1 Quantum Theory and General Relativity

Quantum theory and general relativity are two very different theories. The first, quantum theory, describes microscopic phenomena and the second, general relativity, explains macroscopic behaviour. The two theories are irreconcilable as is, since one is quantised whereas the other is continuous.

In between these two theories there is an interesting regime which is not yet well known. This regime holds an upper bound of quantum mechanics and a lower bound of general relativity. Currently the record for the particle in superposition with the largest effective mass is five milligram [1]. This thesis focusses on the lower bound of general relativity in the Newtonian limit.

The gravitational coupling is smaller than every other coupling via fundamental forces. In order to be able to measure relative small couplings in a system, a resonator can be used. In a resonating system, energy can be added at every cycle, but there will always be energy losses. A low dissipation is necessary in this experiment, this is defined by the Q factor. The Q factor is proportional to the ratio between the energy of a resonance mode and the dissipated energy per cycle in that mode. The Q factor is discussed later on in the theory (chapter 2).

1.2 Measuring Gravity on Small Particles

Recently gravitational coupling was measured between two gold spheres having a radius of 1 mm and a mass of 90 mg, by M. Aspelmeyer et al. [2], which is the lowest bound of general relativity so far. The experiment in this thesis is based on an idea introduced by A. Vinante and H. Ulbricht et al. [3] In this thesis the idea of a levitating particle is used from Vinante et al. The contribution of this thesis is to measure the gravitational coupling between a particle with a mass of roughly 1.5 mg and a brass block of 2.4 kg. The smaller mass is confined in all dimensions such that it is levitating and resonating.

1.2.1 Resonators

For sensitive measurements resonators are used. These resonators are based on the principle of applying a time varying potential at the eigenfrequency of the resonator. This ensures a large amplitude for this mode if this is done for long enough time. The larger the amplitude the easier the detection of the motion is as a rule, but this depends on the detection method.

1.2.2 Membranes

In measurements with resonators (optical) membranes are often used. The membrane acts as a resonator and usually a laser or sometimes a capacitative coupled SQUID (Superconducting Quantum Interference Device) is used to detect the motion. These membranes are strained in a surrounding frame. Because of the straining forces there are always clamping losses. This results in a damped oscillator. In membranes Q factors can reach up to 10^9 and resonance frequencies can be on the lower bound in the MHz regime. [1]

1.2.3 Optically Levitated Particles

Optically levitated particles are trapped in a potential well of a coherent light beam. One degree of freedom is cooled by lowering the amplitude of its motion in that direction/rotation using optical techniques. If the amplitude is low, the effective temperature of this degree of freedom is low. This automatically means not all degrees of freedom have the same temperature.

The degrees of freedom except for the cooled one do contain a lot of energy. The energy ensures a large amplitude. This combined with the states not being perfectly orthogonal causes appreciable cross terms between the degrees of freedom. This leads to energy leaking into the cooled degree of freedom. The leaking of energy causes the amplitude to enlarge and this adds noise to the experiment of measuring gravity.

1.2.4 Levitating Particles

In order to reduce the damping a levitating particle can be used. Levitation ensures very few losses and therefore low damping. On top of that there is no active feedback required to let the levitating particle resonate. The experiment uses a magnet levitating above a superconducting surface. The experiment takes place in a vacuum chamber to eliminate air friction. The main damping left in our system is by Eddy currents at the surface of the superconductor.

According to our calculations it is possible to use a levitating magnet to measure gravity. This calculation is based on a magnet in the order of milligrams and a rotating mass in the order of kilograms. The distance between the two masses is in the order of decimeters. The expected force is in the order of femtonewtons.

The theory chapter provides all necessary theory to understand the experiment. The methods chapter describes the approach of the experiment in practical terms, the design of the superconducting trap, the design of the spinning masses and the expected gravitational force due to the masswheel, moon and the tides of the sea. The results chapter contains the measured results. To end the thesis the discussion and conclusion of the results are provided together with an outlook how to improve the experiment in the future.

Chapter 2

Theory

In this chapter all necessary theory is provided to understand the experiment. Mechanical resonators, the Meissner effect, London penetration depth, interacting magnetic dipoles and energy coupling are the main topics in this chapter. These topics together form the basis of understanding how a magnet can levitate in a superconducting trap, which eigenfrequencies are expected and which magnetic flux is expected to be detected. As described in the introduction, magneto-mechanical resonators are used in this experiment.

2.1 Mechanical Resonators

A resonator is a system in which a restoring force gives rise to an oscillation of some degree of freedom. In the case of a levitating magnet there are three translational and three rotational degrees of freedom which all have their own restoring force. Usually, this restoring force is characterised by a trapping potential.

2.1.1 Trapping Potential

The trapping potential of a mechanical resonator characterises the restoring force with respect to the equilibrium position. If an external force is applied or temperature deviations occur, the oscillator deviates from its equilibrium position and starts to oscillate.

The trapping potential can originate from different kinds of feedback loops. There are two main categories, active and passive feedback loops. In an active feedback loop, feedback is actively provided, that means for example in a potential well of a coherent light beam the potential needs to be actively adjusted. These adjustments are never perfect and will introduce noise to the potential and therefore this is not an ideal solution for a sensitive resonator. In a passive feedback loop, feedback is passively provided. The system itself provides the feedback and there is no feedback source from outside of the system required. The system itself will not introduce noise to the trapping potential because that is only possible if energy is added to the system. A Meissner levitating

particle inside a superconducting trap is an example of a system with passive feedback in the trapping potential. In the next section the Meissner effect is discussed.
Another defining characteristic of a resonator is how long these oscillations persist after being driven. This characteristic is defined by the Q factor.

2.1.2 Q factor

For a damped harmonic oscillator the Q factor is a measure of the damping of the resonator. It is proportional to the ratio between the energy of a resonance mode and the dissipated energy per cycle in that mode. This also means that Q factors of different modes are independent, except if there is coupling between modes via appreciable cross terms at large amplitudes. A lower damping factor results in a higher Q factor. The Q factor is defined by the eigenfrequency of the mode (ω_0) and the damping factor (Γ) or by the damping time (τ), which is defined by the other two properties.

$$Q = 2\pi \times \frac{\text{energy stored}}{\text{energy lost per cycle}} = \frac{\omega_0}{\Gamma} = \frac{2}{\tau} = \frac{1}{2}\omega_0\tau \tag{2.1}$$

The Q factor is not only defined by the stored energy as above, but it also has a definition using the bandwidth. Both definitions are not exactly equal, but for large Q they are approximately equivalent. The used resonating system has a very weak damping and thus both definitions can be used. The definition according to the bandwidth is given below.

$$Q = \frac{\omega_0}{\Delta\omega} = \frac{f_0}{\Delta f} \tag{2.2}$$

In this equation ω_0 and f_0 are respectively the angular resonance frequency and the resonance frequency. The bandwidths are $\Delta\omega$ for the angular bandwidth and Δf for the bandwidth. Both bandwidths are the full width half maximum values at the resonance frequency in the spectrum.

In the case of a levitating magnet, the Q factor together with the mass define the resonating properties of the system. The Q factor acts as a measure of amplification. The Q factor defines the energy losses, if the energy losses are lower than the energy put in the system, the system will be amplified. It depends on the mass how strong the gravitational interaction is. The lighter the mass, the weaker the gravitational interaction, the smaller the energy put in the system per cycle and thus the higher the Q factor needs to be in order to be able to measure gravitational interaction.

2.2 Meissner Effect

The defining property of a superconductor is that an external magnetic field is expelled from the superconductor. This property is called the Meissner effect.
A magnet can levitate above a superconductor using this effect. If a magnet is placed above a superconducting surface, the magnetic field is pushed out of the superconductor. This is done via an induced Eddy current creating a magnetic dipole on the surface of

the superconductor. This results in a repelling force on the magnet. If the magnet is placed vertically above the superconductor (w.r.t. the earth) the gravitational force and the force due to the Meissner effect will balance out such that the magnet levitates. In figure 2.1 an example of a levitating magnet is shown, the magnetic repulsion and the gravitational force are cancelled out.

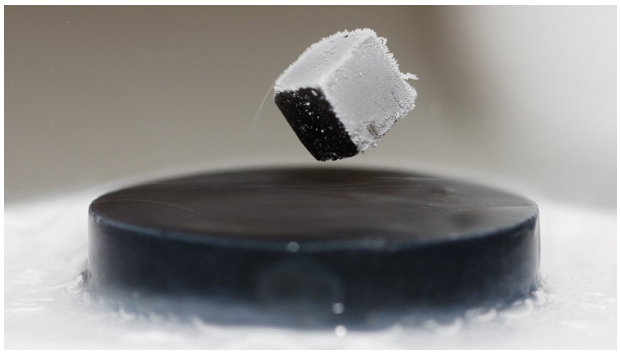

Figure 2.1: *A magnet levitating above a superconductor. Image adapted from Mini Physics [4].*

In the case of a magnet levitating above a superconducting surface, the superconducting surface effectively acts as a mirror for magnetic fields. In the case of a magnet levitating inside of a superconducting trap this mirror effect ensures not only the vertical levitation but also the lateral confinement. This confinement is caused by a trapping potential in the lateral plane and causes a force in the lateral plane which creates the lateral oscillating behaviour.

2.2.1 Types of Superconductors

Two types of superconductors exist, type I and type II. Type I has a single critical magnetic field. Above this critical field all superconducting properties are lost and below this critical field the magnetic field is completely expelled from the superconductor. Type II has two critical fields, between these two fields partial penetration of the magnetic field is possible through vortices. Outside the region between the two critical fields type II superconductors behave the same as type I superconductors for our experiment in bulk magnetic field.

Vortices in type II superconductors make it possible for the magnet to be flux pinned. This means effectively that the magnet is held in place by quantized flux in the superconductor. Flux pinning adapts the trapping potential and it affects the trapping forces. This results in changing of eigenmodes of the resonator. Besides this effect, an oscillating magnet scatters the vortices. Scattered vortices transfer some of their energy in heat and thus create an additional damping factor for the resonator. Both effects are the reason that for this experiment a type I superconductor is used.

In this experiment lead is chosen as the type I superconductor of which the trap is made. The reason this metal is chosen is that it has to be a type I superconductor and for the experiment it is preferred to have a critical temperature above 4.2K. This

makes it possible to do the experiment at liquid helium-4 temperatures. With these two requirements there are few metals left. Lead is the only metal on this list which can practically be used to make the desired traps.

2.3 London Penetration Depth

If a superconductor is placed in a magnetic field some of the field will always penetrate in the superconductor. The London penetration depth is a measure of the distance at which the magnetic field inside the superconductor is equal to $\frac{1}{e}$ of the magnetic field at the surface of the superconductor.

The London penetration depth can be calculated as follows:

$$\lambda_L = \sqrt{\frac{m}{\mu_0 n q^2}} \tag{2.3}$$

Where m is the mass of the charge carriers, μ_0 is the magnetic permeability, n is the number density of free electrons in the superconductor and q is the charge of the charge carriers. An experimental value for the penetration depth in lead can be found in McLean [5], the value is: $\lambda_L = 30.5\,\mathrm{nm}$ at $T = 0\,\mathrm{K}$.

The London penetration depth also depends on the temperature of the superconductor. During this experiment the temperature was 200 mK or less. The critical temperature of lead is $T_c = 7.2\,\mathrm{K}$ [5]. In equation 2.4 the relative deviation between the penetration depth at temperature T and temperature 0 K is shown in parts per million. In this equation $\lambda(0)$ is the value of the penetration depth at $T = 0\,\mathrm{K}$ and $\lambda(T)$ is the penetration depth at temperature T. The relative deviation of the penetration depth at 200 mK is calculated since this is an upper bound during the experiment.

$$\frac{\Delta\lambda}{\lambda(0)} = \frac{\lambda(T) - \lambda(0)}{\lambda(0)} = \left[\frac{1}{\sqrt{1-(T/T_c)^4}} - 1\right] \cdot 10^6 \mathrm{ppm} \tag{2.4}$$

$$= \left[\frac{1}{\sqrt{1-(200\,\mathrm{mK}/7.2\,\mathrm{K})^4}} - 1\right] \cdot 10^6 \mathrm{ppm} = 0.30\,\mathrm{ppm} \tag{2.5}$$

It can be concluded that the value for the penetration depth does not significantly change during the experiment.

2.3.1 Magnetic Field on the Superconducting Surface

Besides a critical temperature, a superconductor also has a critical magnetic field. If this field is exceeded the superconductor will be a normal conductor again. Due to the process of magnetising a ferromagnet, a ferromagnet always has a remnant magnetic field (B_r). In Neodymium magnets this value can reach up to 1.3 T, in the calculations in this thesis this upper bound or a conservative value of 700 mT is used depending on the purpose of the calculation.

The magnetic field parallel to the magnetization axis is twice as large as the magnetic field perpendicular to this axis. In section 3.3.1 the design for our trap, lake Ontario, and in section 3.3.3 the used magnet are discussed. Some dimensions mentioned in these sections are used in this calculation. In lake Ontario the short axis is $L_x = 3.5\,\mathrm{mm}$ and the long axis is $L_y = 4.5\,\mathrm{mm}$. The length of the magnet is 1 mm and the diameter is about 0.5 mm. This means in the x-direction there is 1.50 mm free space on both sides and in the y-direction there is 1.75 mm.
The magnetic field of a dipole can be written as an inner vector product of the magnetic moment and the position unit vector [6]. If cylindrical coordinates are used and the magnetic moment is aligned with the z-axis, the magnetic field can be expressed as in equation 2.7.

$$\mathbf{B}(\mathbf{r}) = \frac{\mu_0}{4\pi}\left[\frac{3\hat{\mathbf{r}}(\mathbf{m}\cdot\hat{\mathbf{r}}) - \mathbf{m}}{r^3}\right] \tag{2.6}$$

$$= \frac{\mu_0|m|}{4\pi r^3}\left(2\cos\theta\ \hat{\mathbf{r}} + \sin\theta\ \hat{\boldsymbol{\theta}}\right) \tag{2.7}$$

The angle θ is the angle measured from the positive z-axis. The field in the positive and negative z-axis direction is twice as strong as in the $\theta = 90°$ direction. In this relation it be can seen that the field decays with r^3.
The x-direction is chosen to be the short axis of the elliptically shaped trap, where the angle $\theta = 90°$. At the superconducting surface in the x-direction the upper bound of the field is:

$$B_{\mathrm{x,\ surface}} = B_r\left(\frac{x_{\mathrm{radius}}}{x_{\mathrm{surface}}}\right)^3 = 1.3\,\mathrm{T}\left(\frac{0.25\,\mathrm{mm}}{1.75\,\mathrm{mm}}\right)^3 = 3.8\,\mathrm{mT} \tag{2.8}$$

Where x_{radius} is the distance from the centre of the magnet to the surface of the magnet, this is 0.25 mm. In this case x_{surface} is the distance from the centre of the magnet to the surface of the superconductor, this is 1.75 mm.

For the y-direction the same field strength can be calculated. In the y-direction the angle $\theta = 0°$ and the field is twice as large here as in the x-direction.

$$B_{\mathrm{y,\ surface}} = 2B_r\left(\frac{y_{\mathrm{radius}}}{y_{\mathrm{surface}}}\right)^3 = 2\cdot 1.3\,\mathrm{T}\left(\frac{0.5\,\mathrm{mm}}{2.25\,\mathrm{mm}}\right)^3 = 29\,\mathrm{mT} \tag{2.9}$$

In this case, y_{radius} is 0.5 mm and y_{surface} is 2.25 mm.
The critical field of lead is 80 mT, so both calculated fields are well below the critical field. Therefore the chance of the lead leaving the superconducting state is neglectable if the magnet is near the equilibrium position.

Critical Distance

The critical magnetic field can also be used the other way around. The distance between the magnet and the surface of the superconductor can be calculated at which the

superconductor loses its superconducting state.

$$r_{\text{critical, x}} = r_{\text{radius}} \left(\frac{B_r}{B_{\text{critical}}} \right)^{1/3} = (0.25\,\text{mm}) \left(\frac{1.3\,\text{T}}{80\,\text{mT}} \right)^{1/3} = 0.63\,\text{mm} \tag{2.10}$$

This is the value for the field in the x-direction, for the y-direction a factor two needs to be added to the remnant magnetic field and the correct value for the radius has to be used. This results in $r_{\text{critical, y}} = 1.6\,\text{mm}$.
This means that if the center of the magnet is closer than 0.63 mm in the x-direction or 1.6 mm in the y-direction to the surface of the superconductor, the superconductor will lose its superconducting properties. Since half the length of the magnet in the x-direction is 0.25 mm, the distance between the magnet and the superconductor can be 0.38 mm in this direction. In the y-direction half the length is 0.5 mm and thus the distance between the two surfaces can be 1.1 mm.
For the z-direction the levitation height determines the distance between the magnet and the superconductor. Because of the symmetry of the magnet, the critical distance in the z-direction is the same as in the x-direction. Both axes have a magnetic field perpendicular to the magnetization axis and the magnet has the same length in the z-direction as in the x-direction. Therefore the critical distance in z-direction is also 0.63 mm from the center of the magnet to the superconducting surface. For a distance of less than 0.38 mm between the surface of the magnet and the surface of the superconductor the superconductor will lose its superconducting properties.

These conditions define the minimal thickness of the superconducting potential well. If one of the superconducting walls does not obey the minimal thickness and the magnet is placed against this wall during the cool down the magnetic field will be frozen in the superconductor. This pins the magnet at this position and so it will not levitate and it will be pinned. This problem can be prevented by just having walls thicker than the critical lengths.

2.3.2 Eddy Currents

At the surface of the superconductor there is a penetration depth in which the metal will have a normal state, so there it is no superconductor. Because this layer is in a normal state, Eddy currents occur if there is a magnetic field present. In the case of a magnetic levitating particle it will ensure there is a magnetic field present in the superconducting trap. The Eddy currents will act as a damping force on the motion of the levitating magnet. In the master thesis of Jean-Paul van Soest [7] this is discussed in paragraph 2.5.2.

2.4 Interacting Magnetic Dipoles

The surface of the superconductor carries Eddy currents, these act as a mirror for magnetic fields. Using this statement the superconductor can be modelled from the magnet's point of view by image dipoles. The magnetic interaction Hamiltonian is used to calculate the eigenfrequencies, spring constants and equilibrium positions in all dimensions.

2.4.1 Magnetic Interaction Hamiltonian

The Hamiltionian for two interacting dipoles is given in Griffiths [6] as:

$$H = -\frac{\mu_0}{4\pi\,|\mathbf{r}|^3}\left(3(\boldsymbol{\mu_1}\cdot\hat{\mathbf{r}})(\boldsymbol{\mu_2}\cdot\hat{\mathbf{r}}) - \boldsymbol{\mu_1}\cdot\boldsymbol{\mu_2}\right) + \mu_0\frac{2}{3}\boldsymbol{\mu_1}\cdot\boldsymbol{\mu_2}\delta(\mathbf{r}) \tag{2.11}$$

Where $\mathbf{r}$ is the distance vector between the two dipoles and $\boldsymbol{\mu_i}$ is the magnetic moment of particle i. The last term vanishes everywhere but the origin, this term ensures that $\nabla\cdot\mathbf{B} = 0$ everywhere.

2.4.2 Vertical Mode

The vertical mode is different from the lateral modes. The vertical mode is bound by the bottom of the trap and by gravity. The lateral modes are bound by the walls of the trap surrounding the magnet. First the Hamiltonian for the interaction between the magnet and the bottom of the trap is calculated. This interaction is in the vertical ($\hat{z}$) direction. The magnet can also rotate in the vertical direction. The vertical rotation around its center of mass is defined by an angle (β), as defined in figure 2.2.

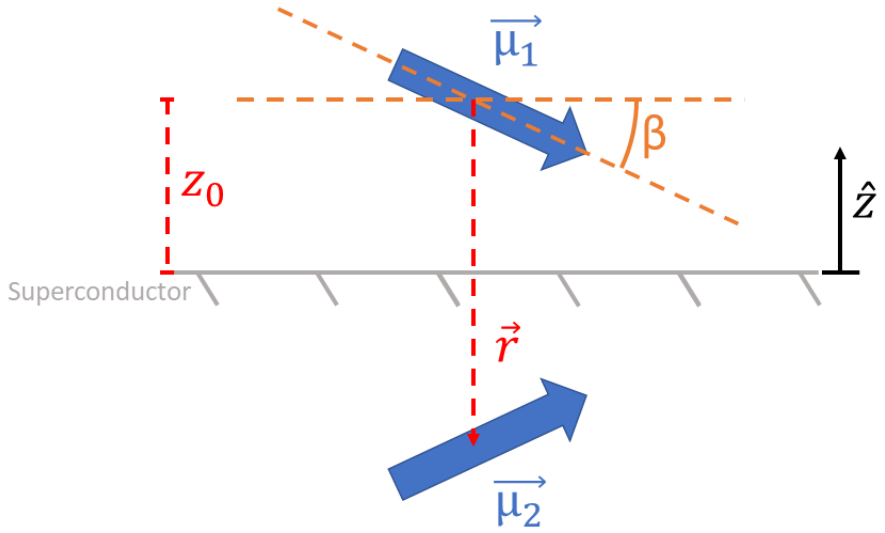

Figure 2.2: *A schematic image where the real magnet dipole ($\boldsymbol{\mu_1}$) and the mirrored image dipole ($\boldsymbol{\mu_2}$) are illustrated. The two dipoles are separated by a distance vector ($\mathbf{r}$), half this distance is the levitation height (z_0). The surface of the superconductor is shown as a mirror. The direction of the z-axis is shown.*

Figure 2.2 shows the rotational angle (β) and two magnetic moments, the real dipole of the magnet ($\boldsymbol{\mu}_1$) and the mirrored image dipole ($\boldsymbol{\mu}_2$). The dipoles are separated by a distance vector ($\mathbf{r}$), half this distance is the levitation height (z_0). These definitions are now used to derive the Hamiltonian in the vertical direction.

$$H = -\frac{\mu_0}{4\pi |\mathbf{r}|^3}\left(3\mu_1|\hat{r}|\cos(\frac{\pi}{2}-\beta)\cdot\mu_2|\hat{r}|\cos(\frac{\pi}{2}+\beta)-\mu_1\mu_2\cos(2\beta)\right) \tag{2.12}$$

$$= -\frac{\mu_0}{4\pi |\mathbf{r}|^3}\left(3\mu_1\mu_2\frac{1}{2}\left[\cos(-2\beta)+\cos(\pi)\right]-\mu_1\mu_2\cos(2\beta)\right) \tag{2.13}$$

$$= -\frac{\mu_0}{4\pi |\mathbf{r}|^3}\left(\frac{1}{2}\mu_1\mu_2\cos(2\beta)-\frac{3}{2}\mu_1\mu_2\right) \tag{2.14}$$

$$= -\frac{\mu_0}{4\pi |\mathbf{r}|^3}\frac{1}{2}\mu_1\mu_2(\cos 2\beta - 3) \tag{2.15}$$

$$= -\frac{\mu_0}{4\pi |\mathbf{r}|^3}\frac{1}{2}\mu_1\mu_2(2\cos^2\beta - 4) \tag{2.16}$$

$$= \frac{\mu_0\mu_1\mu_2}{4\pi |\mathbf{r}|^3}(\sin^2\beta + 1) \tag{2.17}$$

This obtained result is the interaction energy between two real magnetic dipoles. In the image method however one dipole is real and the other one does not exist, it is created by Eddy currents on the surface within the London penetration depth. The field at the position of the real dipole is created by Eddy currents and can be seen as an image dipole. Because of this reason the effective potential energy is exactly $\frac{1}{2}\boldsymbol{\mu}\mathbf{B}$ [8]. Where $\boldsymbol{\mu}$ is the real dipole and $\mathbf{B}$ is the image field.

The reason above causes an additional factor of one half to be added to equation 2.17. For the potential in the z-direction, gravity also needs to be taken into account. Furthermore the distance between the magnet and the superconducting surface (z) is half of the distance between the two dipoles ($|\mathbf{r}|$), or in a formula: $|\mathbf{r}| = 2z$. The final vertical potential energy is now given by:

$$U_z = \frac{\mu_0\mu_1\mu_2}{64\pi z^3}(\sin^2\beta + 1) + mgz \tag{2.18}$$

Levitation Height

As calculated in equation 2.18, the potential energy of the vertical mode is known. Using this, the levitation height (z_0) can be determined. At this height there is an equilibrium between the magnetic repulsion and the gravitational attraction of the magnet and the earth. This equilibrium height or levitation height is equal to the derivative of this potential with respect to z equated to zero. This derivative is equal to the force in the z-direction.

$$F_z = -\frac{dU_z}{dz} = \frac{3\mu_0\mu_1\mu_2}{64\pi z^4} - mg = 0 \tag{2.19}$$

Solving for z, this results in the levitation height (z_0):

$$z_0 = \left(\frac{3\mu_0\mu_1\mu_2}{64\pi mg}\right)^{1/4} = \left(\frac{3B_r^2V_1V_2}{64\pi\mu_0 mg}\right)^{1/4} \tag{2.20}$$

Using the values from the methods section, the levitation height is calculated at $z_0 = 2.0\,\mathrm{mm}$.

Vertical Eigenfrequency

The potential energy and the levitation height have been derived. They can be combined to calculate the spring constant and the eigenfrequency in the vertical direction. The second derivative of the potential energy with respect to z is taken and the levitation height is chosen as the equilibrium position for the oscillation.

$$k_z = \left.\frac{d^2U_z}{dz^2}\right|_{z_0} = \frac{3\mu_0\mu_1\mu_2}{16\pi z_0^5} = \frac{3B_r^2V_1V_2}{16\pi\mu_0 z_0^5} \tag{2.21}$$

This results in a vertical spring constant of $k_z = 0.029\,\mathrm{N/m}$.

Now the vertical spring constant is known so the vertical eigenfrequency can be calculated.

$$\omega_z = \sqrt{\frac{k_z}{m}} \tag{2.22}$$

This gives $\omega_z = 138\,\mathrm{rad/s}$ as the angular eigenfrequency in the vertical direction. This is equal to a frequency of $f_z = 22\,\mathrm{Hz}$.

Vertical Rotational Eigenfrequency

For the rotational mode (β) the same method as for the vertical eigenmode can be used to determine the spring constant and the eigenfrequency.

Two possibilities for the equilibrium angle (β_0) exist. The first one is $\beta = 0°$ and second is $\beta = 90°$. Since the particle is asymmetric the case of 0° will be stable and 90° unstable, thus the equilibrium angle will be $\beta_0 = 0°$.

$$k_\beta = \left.\frac{d^2U_z}{d\beta^2}\right|_{z_0,\beta_0} = \frac{\mu_0\mu_1\mu_2}{32\pi z_0^3}\left(\cos^2\beta_0 - \sin^2\beta_0\right) \tag{2.23}$$

$$= \frac{B_r^2V_1V_2}{32\pi\mu_0 z_0^3}\left(\cos^2\beta_0 - \sin^2\beta_0\right) \tag{2.24}$$

The resulting rotational spring constant is: $k_\beta = 22\times10^{-9}\,\mathrm{Nm}$. The frequency is calculated using the rotational spring constant and the moment of inertia.

$$\omega_\beta = \sqrt{\frac{k_\beta}{I}} \tag{2.25}$$

The used magnet is approximately a cylinder as described in section 3.3.3, the radius and length are also used from the same section. The moment of inertia for a cylinder is: $I = \frac{1}{2}mr^2 + \frac{1}{12}ml^2 = 1.7\times10^{-13}\,\mathrm{kg\ m^2}$. This results in a vertical rotational angular eigenfrequency $\omega_\beta = 386\,\mathrm{rad/s}$ and is equal to a vertical rotational frequency of $f_\beta = 61\,\mathrm{Hz}$.

2.5 Flux Position Dependence

The oscillating magnet will create a changing flux in a detection coil. This detection coil creates a current in a superconducting circuit; consisting of the detection (or pickup) coil (2.3 nH), the SQUID input coil (400 nH), and the calibration transformator (4.4 nH). Via the SQUID input coil, the motion of the magnet can be detected. The calibration transformation coil is used to calibrate the motion of the magnet.

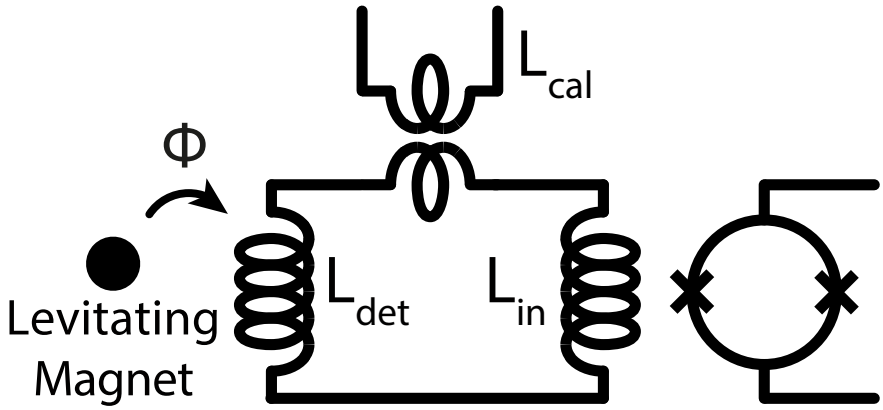

Figure 2.3: *The electric circuit is shown. The magnet oscillates and creates a changing flux in the detection (or pickup) coil (*2.3 nH*). Via the SQUID input coil (*400 nH*) the changing flux is detected. A calibration transformator (*4.4 nH*) is included to calibrate the motion of the magnet. The total inductance is* 407 nH*. Image adapted from the Oosterkamp group.*

To calculate the magnetic flux (Φ) in a coil, the following equation is used:

$$\Phi = NAB_{\perp} \tag{2.26}$$

Where N is the number of windings of the wire the coil consist of, A is the surface area of the coil and $B_{\perp}$ is the magnetic field perpendicular to the surface of the coil. For an oscillating magnet the flux will change with the position. The derivative with respect to the position can be taken.

$$\frac{d\Phi}{dx} = NA\frac{dB_{\perp}}{dx} \tag{2.27}$$

The magnetic field in this calculation is approximated as spherical shells. This approximation is less correct at the poles than on the equatorial plane of the magnet. Using this approximation and the angle defined in figure 2.4 the field in the pickup coil is:

$$\frac{dB_{\perp}}{dx} \simeq \sin\theta\frac{dB(r)}{dr} \tag{2.28}$$

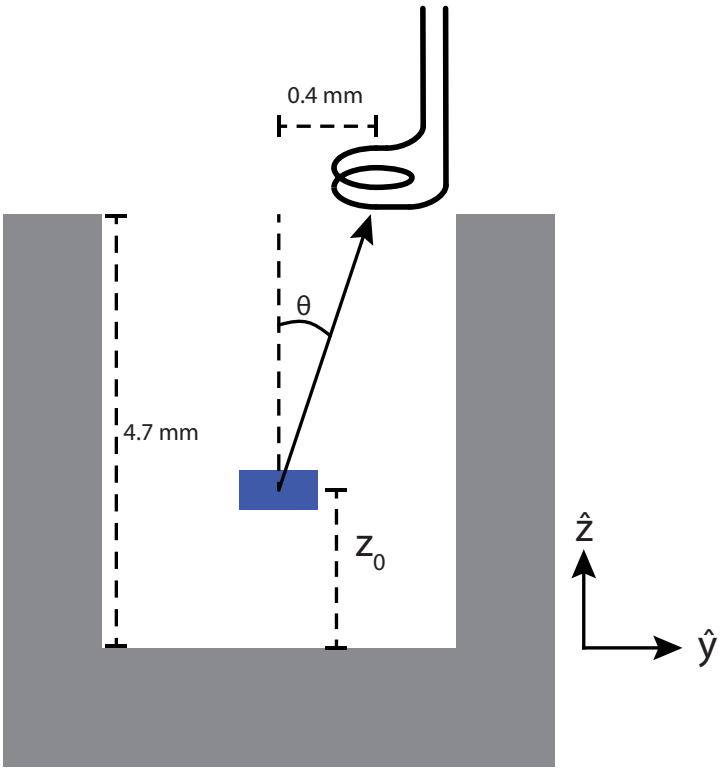

Figure 2.4: *A schematic overview of the magnet (in blue) levitating inside the trap (gray). In this figure the angle θ is defined between the vertical and the direction of the pickup coil. The inner height is* 4.7 mm *as given in section 3.3.1.*

As depicted in figure 2.4 the angle θ is: $\sin\theta = \frac{0.4}{\sqrt{(4.7-2.0)^2+0.4^2}} = 0.147$
The remnant magnetic field in the vertical direction is $B_r = 700\,\mathrm{mT}$. For the spherical approximation this gives a radial dependence of:

$$B(r) = B_r \frac{a^3}{r^3} \tag{2.29}$$

Where a is the spherical radius of the magnet. The used magnets are actually cylindrical, the magnetic field approximation however will not be affected much by this, since the pickup coil is more than six radii away from the magnet.
To continue with the calculation of the flux position dependence, the derivative with respect to r is calculated.

$$\frac{dB(r)}{dr} = -\frac{3}{2} B_r \frac{a^3}{r^4} \tag{2.30}$$

Now the flux position dependence can be determined. This is done by filling in the

obtained results in equation 2.27.

$$\frac{d\Phi}{dx} \simeq -\frac{3}{2} NAB_r \sin\theta \frac{a^3}{r^4} \tag{2.31}$$

The values for each of the variables can be found in section 3.3. Using these values the theoretical maximal value for the flux position dependence is calculated as: $\frac{d\Phi}{dx} \simeq -6.8 \cdot 10^{-8} \frac{Tm^2}{m}$.

2.6 Energy Coupling

The magnet can be magnetically driven via the calibration coil. The flux created in the calibration coil creates a current and thus creates a flux in the pickup coil and in the SQUID input coil. The flux in the pickup coil influences the oscillation of the magnet. This can be used to measure the energy coupling. The energy coupling is the ratio between the energy in the electrical system and the kinetic energy of the oscillating magnet. The energy coupling is independent for every resonance frequency.

If a current is injected via the calibration trafo, the flux can be measured in the SQUID, on top of this flux there is also a flux of the oscillating magnet. The oscillating magnet has a different phase than the injected flux, because if the magnet goes through its resonance frequency the phase is rotated by 180°. These effects are independent for every resonance frequency and therefore this process needs to be done for every mode individually. By definition the ratio between the particle flux and the flux due to the drive is: $\Phi_{\text{drive}}/\Phi_{\text{particle motion}} = Q \cdot \beta^2$. Here β^2 is the energy coupling, β is the transfer function.

In figure 2.5 the modulus and the phase of the transfer function are plotted in the complex plane. As described above the phase rotates by 180° at the resonance frequency. The modulus has a dip around the resonance frequency. The combination of these two creates a circle in the complex plane of the transfer function. This is depicted in figure 2.5. The ratio between the crosstalk (vector κ) and the motion of the particle (vector ξ) is: $\kappa/\xi = Q\beta^2$.

The energy coupling quantizes how much of the energy in the electrical system is transferred to kinetic energy of the magnet. The energy coupling works in both ways, the energy in the electrical system is coupled to the motion of the magnet and the motion of the magnet is coupled to the electrical system. Below the energy coupling is given as a fraction of the energy in the system and the kinetic energy.

$$\beta^2 = \frac{E_{\text{system}}}{E_{\text{kin}}} \tag{2.32}$$

In this equation E_{system} is the energy in the electrical system. It contains a component in the pickup coil, one in the SQUID input coil, one in the calibration coil and a possible resistance in the wires (if they are not superconducting). The kinetic energy of the magnet is E_{kin}.

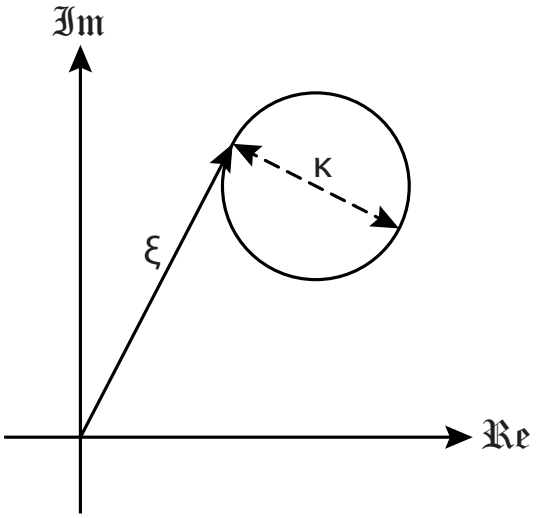

Figure 2.5: *The transfer function around the resonance frequency is plotted in the complex plane. Around the resonance frequency the phase rotates by 180°. The modulus of the transfer function has a dip around the resonance frequency. The ratio between the two vectors is $Q\beta^2$.*

For a coil in general the energy in the coil (E_{coil}) is known.

$$E_{\text{coil}} = W_{\text{coil}} = \frac{1}{2} L_{\text{tot}} I^2 \tag{2.33}$$

In this electrical circuit the total inductance is: $L_{\text{tot}} = L_{\text{pickup loop}} + L_{\text{calibration coil}} + L_{\text{SQUID}}$. The inductance and the magnetic flux are related as follows:

$$\Phi = LI \tag{2.34}$$

These equations result in the coil energy:

$$E_{\text{coil}} = \frac{1}{2} I\Phi = \frac{1}{2} \frac{\Phi^2}{L_{\text{tot}}} \tag{2.35}$$

The kinetic energy of the magnet is given by the expression for a harmonic oscillator. The magnet will oscillate periodically in time and it can be described using a quadratic potential.

$$E_{kin} = \frac{1}{2} m\omega^2 x^2 \tag{2.36}$$

Both the kinetic and the coil energy are used to find an expression for the energy coupling.

$$\beta^2 = \frac{\frac{1}{2}\frac{\Phi^2}{L}}{\frac{1}{2} m\omega^2 x^2} = \frac{\Phi^2}{x^2} \frac{1}{L_{\text{tot}} m\omega^2} \tag{2.37}$$

The magnet is oscillating and thus the position of the magnet changes. The pickup loop is fixed so a change in position is proportional to a change in flux. With this in mind the changing position and changing flux can be integrated in the energy coupling.

$$\beta^2 = \frac{\delta\Phi^2}{\delta x^2}\frac{1}{L_{\text{tot}} m\omega^2} \tag{2.38}$$

By taking the infinitesimal limit of δx the differentials are obtained.

$$\beta^2 = \left(\frac{d\Phi}{dx}\right)^2 \frac{1}{L_{\text{tot}} m\omega^2} \tag{2.39}$$

Using the previous result of the maximal flux position dependence, the vertical eigenfrequency from section 2.4.2, the total inductance from section 2.5 and the mass of section 3.3.3 the energy coupling is now calculated. This results in: $\beta^2 \simeq 3.6 \times 10^{-7}$

2.6.1 Flux Position Conversion

The energy coupling is used to calculate the conversion factor between the SQUID voltage and the distance of the oscillating magnet. The oscillating magnet creates a flux which is transported via the superconducting loop to the SQUID. This is measured as a voltage on the output of the SQUID. The responsivity of this detection method is adapted from G. Wijts [9] equation 3.9.

$$\frac{dU}{dx} = -\frac{M}{L_{\text{tot}}} V_\Phi \frac{d\Phi}{dx} \tag{2.40}$$

In this equation U is the measured voltage of the SQUID, x is the movement distance of the magnet, M is the mutual inductance between the input coil and the SQUID, L_{tot} is the total inductance of the superconducting loop and V_Φ is the gain of the SQUID in V/Wb. Now, equation 2.39 is used to get a result in terms of measurable parameters.

$$\frac{dU}{dx} = -\frac{M}{L_{\text{tot}}} V_\Phi \sqrt{\beta^2 L_{\text{tot}} m\omega^2} \tag{2.41}$$

$$\frac{dx}{dU} = -\sqrt{\frac{L_{\text{tot}}}{m\beta^2}} \frac{1}{MV_\Phi 2\pi f} \tag{2.42}$$

In the last equation (2.42) the angular frequency is replaced by the frequency using: $\omega = 2\pi f$. This is done because during measurements the frequency f will be measured and not the angular frequency.

Chapter 3

Method

Using the now known theory, various methods are introduced to eventually measure a Meissner levitating magnet. As discussed in the theory, the experiment takes place at cryogenic temperatures. The working principle of a cryostat and its vibration isolation are explained. In order to measure the magnetic flux, the working principle of a SQUID is briefly explained.

For this experiment specifically the design and properties of our trap, Lake Ontario, are given. The wheel with rotating masses is characterised and how the vibrations of the wheel are damped is discussed.

In the last part of this chapter it is discussed how several things are measured. It is explained how to know if a particle levitates and how to know if the exerted force on the particle is due to gravitational interaction. The feasibility of measuring gravitational interaction in our set-up is simulated. As a side project the options for measuring the gravity by the moon and the tidal action of the seawater are discussed.

3.1 Cryostat

In this experiment the used cryostat is a closed-cycle dilution refrigerator. Theoretically this cooling method can reach temperatures as low as 2 mK.

The dilution refrigerator uses a pulse tube to pump gaseous helium-4 through the system. The pulse tube has a cycle where it compresses and decompresses helium-4, the decompression is an endothermic process. This principle takes energy from the system and brings out decompressed helium-4. The used pulse tube is a two stage tube, meaning that it cools the first plate to 50 K and the next plate to 4 K. In practice a temperature of 3.4 K can be reached at the 4 K plate.

To obtain lower temperatures, dilution refrigeration is used. A closed system which goes through the mixing chamber and the still contains ^{4}He. This is cooled down using the pulse tube. Now, ^{3}He is pumped in the same closed system. These two isotopes will mix, this mixing process creates cooling power.

All ^{4}He atoms are bosons and can reach the ground state, the ^{3}He atoms are fermions and cannot reach the ground state due to the Pauli exclusion principle. The mixing of the two isotopes increases the entropy of the mixture, due to the third law of thermodynamics this decreases the entropy of its surroundings and this effectively removes energy from the system. This mixture will reach a thermodynamic equilibrium for 6 vol% ^{3}He and 94 vol% ^{4}He.

At the surface of the mixture in the mixing chamber the ^{3}He atoms will evaporate and they are circulated back into the system. The continuous cycle of the ^{3}He atoms ensures a continuous cooling power. This dilution refrigeration method can theoretically reach temperatures of 2 mK, in practice the used cryostat has a base temperature of 10 mK.

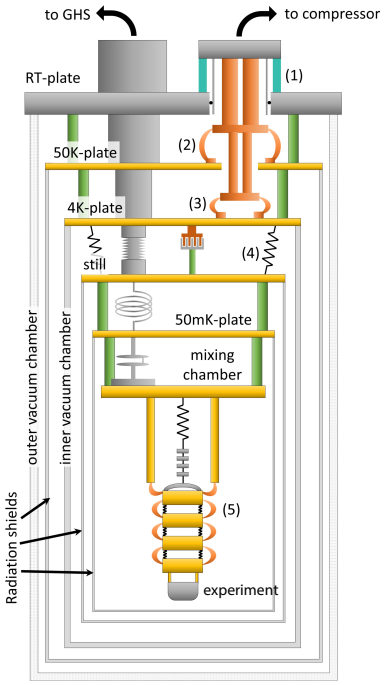

Figure 3.1: *Schematic image of the cryostat. Several components are indicated by a description or a number. This image is adapted from M. de Wit [10]. In the right top the pulse tube is shown in red. It is mechanically isolated from the room temperature plate (1). The heat conductance from the first stage of the pulse tube to the 50 K plate is shown at (2). The same principle is shown at (3) for the 4 K plate. The still (or 1 K plate) is suspended by springs from the 4 K plate, illustrated at (4). The mass spring system is shown at (5). The latter two both contribute to the vibration isolation.*

In figure 3.1 a schematic illustration of the cryostat is given. The vertical plates are shown, each with their own temperature. Starting at the top, first there is the room temperature plate, next the 50 K plate, then the 4 K plate, the still, the 50 mK plate and at the bottom the mixing chamber plate. The plates are enclosed by two vacuum chambers and three radiation heat shields.

3.1.1 Vibration Isolation

The cryostat is vibration isolated from the rest of the building. The cryostat is mounted on a concrete block of 25 tonnes which is on dampers on top of its own piles (separately from the rest of the building). The 1 K plate is suspended by springs from the 4 K plate acting as a mass spring system, this is shown in figure 3.1 at position (4).

A picture of the experiment including the mixing chamber plate is shown in figure 3.2. In the left part (A) the overview is shown, starting at the mixing chamber plate at the top down to the experiment at the bottom. The right part (B) is zoomed in on the hanging part from the long bendable arm and below. The caption highlights the indicated components.

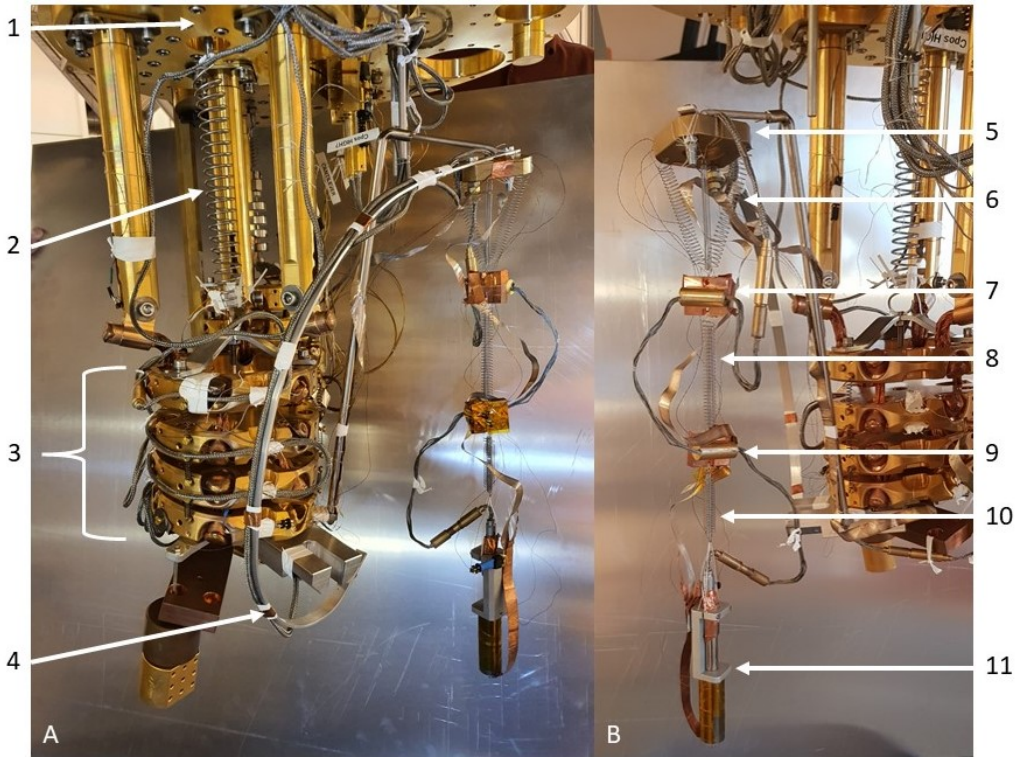

Figure 3.2: *Picture of the experiment. The left side (A) shows the overview of the mixing chamber plate down to the experiment. The right side (B) shows the hanging part from the long bendable arm downwards. Starting at the mixing chamber plate (1) first there is a spring downwards (2), and then a mass spring system (3). This mass spring system consists of four masses with springs in between them and copper heat links for thermalisation. After these stages there is a long bendable arm (4) with a mass on top (5). From this mass there are three springs (6) downward attached to a copper mass (7), this mass has a coaxial spring (8) attached to another copper mass (9) and at last there is a coaxial spring (10) to the experiment (11).*

Every mass spring system adds a damping factor, if the resonance frequency is chosen as such. This is the reason why so many masses and springs are used.

3.2 SQUIDs

The magnetic flux of the oscillating magnet is measured using a SQUID. The amplitude of the oscillation is in the order of nanometres or less, thus a sensible method for detecting magnetic flux is desired. In the experiment a Superconducting Quantum Interference Device (SQUID) is used. A SQUID uses Josephson junctions to measure fractions of magnetic flux quanta.

3.3 Lake Ontario

In the experiment a superconducting trap is used. The traps all have names of lakes in Canada, this trap is called Lake Ontario.

3.3.1 Design

For Lake Ontario an elliptical shape was chosen. This ellipticity ensured that the eigenmodes in the lateral plane are different. In figure 3.3 the schematic design is given. In the left part of the figure the lid is shown and in the right part a vertical intersection is given. The small circle in the middle of the lid is the axis where the pickup coil is wound. Around this axis a coil with two windings is wound for the detection coil and a coil with ten windings (sometimes referred to as the N=10 coil) is wound to make it possible to drive the magnet harder. These coils have a diameter of 1 mm and an intersection of 0.79 mm^2. The axis is 0.4 mm out of center in the y-direction and centered in the x-direction. This coil is out of center to have a larger flux gradient than with the coil in the center of the lid. In the thesis of Van Soest [7] this out of center coil was simulated. It turned out the out of center coil results in a larger energy coupling.

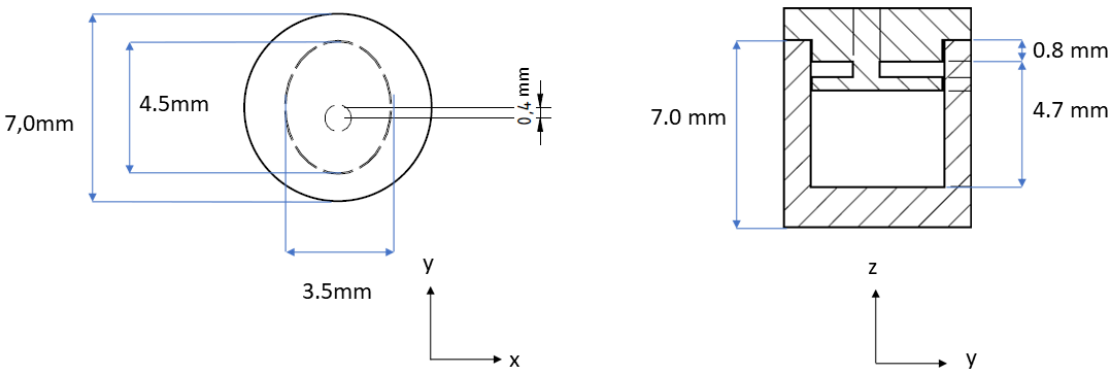

Figure 3.3: *The schematic design of Lake Ontario. Sizes are given in the figure as well as the definition of the axes.*

3.3.2 Fabrication

All parts of Lake Ontario were fabricated by the Fine Mechanics Department (FMD) at Leiden University. The lead trap, the lid, the aluminium holder and the cover are self-made by the FMD.

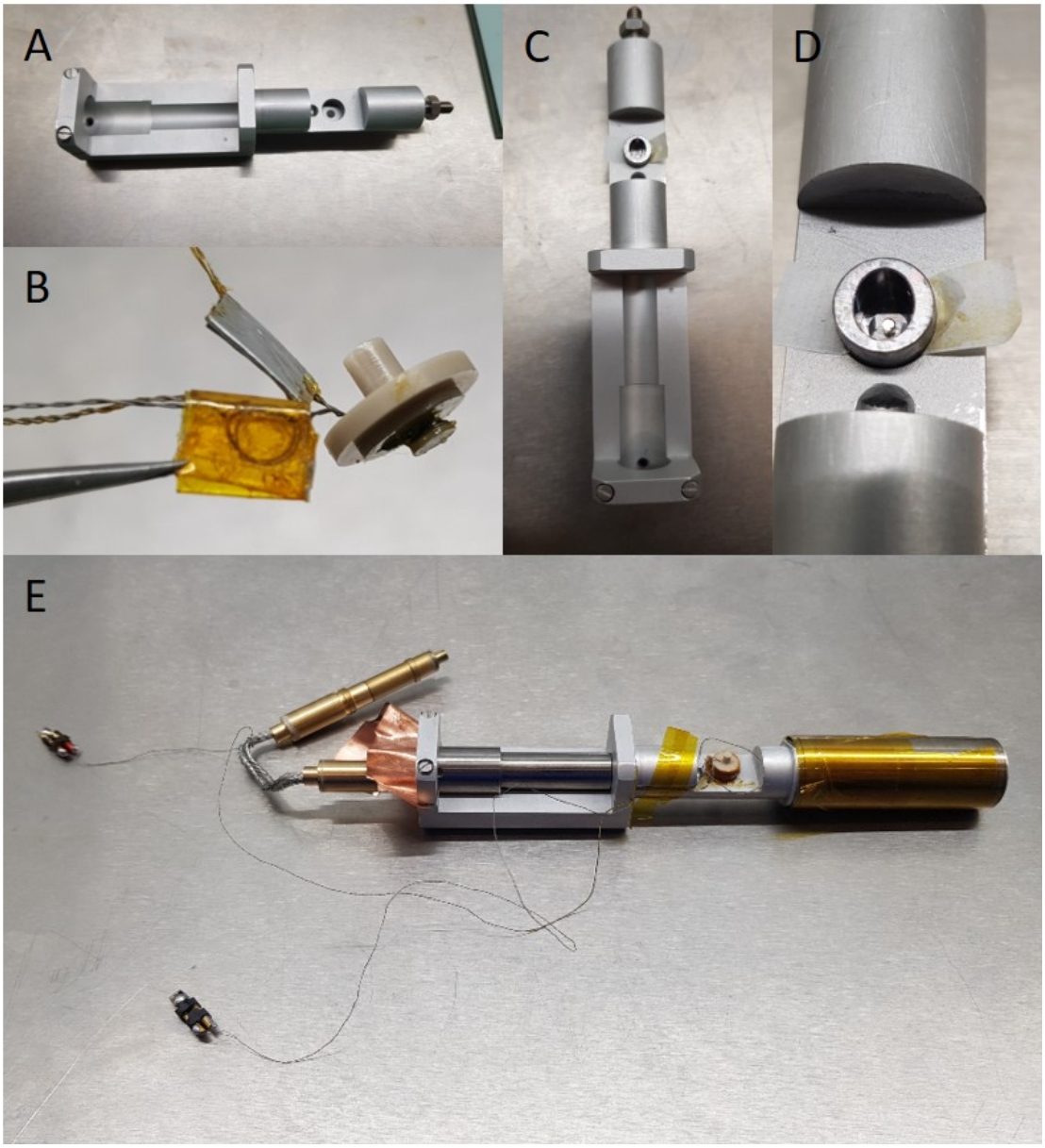

Figure 3.4: *Photos of the different steps in fabricating Lake Ontario. A) The empty aluminium holder. B) The lid including the pickup and the N=10 coil and the calibration transformator. C) The aluminium holder including the lead trap. D) The holder and lead trap with the magnet placed inside. E) The complete set-up, including the SQUID with the cover opened.*

The trap is made out of lead as discussed in section 2.2.1. The lid is made from polyether ether ketone (PEEK), this is a type of plastic which can withstand cryogenic temperatures and it has no magnetisation. The holder is made out of aluminium because aluminium is a superconductor below 1.2 K [11]. During the experiment the set-up will always be below this temperature, therefore as a superconductor the holder will freeze all magnetic field that is left. This does not take away the magnetic field, but it ensures the magnetic field does not change in and around the lead trap.

In figure 3.4 photos of different stages during fabrication are shown. Photo (A) shows the empty aluminium holder. Photo (B) shows the lid with the pickup coil and N=10 coil. In the yellow kapton (polyimide) tape the calibration transformator can be seen. Photo (C) shows the aluminium holder with the lead trap inside, the lead trap was fixed on it's position using GE varnish. Photo (D) shows the magnet inside the lead trap. Photo (E) shows the total set-up, including the SQUID inside the SQUID holder. On the right side of the image the cover is opened to be able to see the inside.

3.3.3 Magnet

The used magnet is ordered at Webcraft GmbH in Germany. The magnet in figure 3.4 is not actually the magnet used in the experiments where all results were obtained. This magnet is cylindrically shaped, with a length and a diameter of 1.0 mm made out of neodymium-iron-boron (NdFeB). The magnet used during the experiments where all results were obtained was a shatter of the magnet in figure 3.4. The shatter was approximately a cylinder with a length of 1.0 mm and a diameter of 0.5 mm. These dimensions and a density of 7600 kg/m^3 were used to calculate the mass as 1.5 mg.

Figure 3.5: *The magnet used in the experiments where all results were obtained. The magnet is approximately cylindrical with a length of* 1.0 mm *and a diameter of* 0.5 mm*. In the lower right there is a cable with a diameter with* 1.0 mm *as a reference. Image was taken under an optical microscope.*

3.3.4 Ventilation Holes

After several tries of the experiment it was thought that the lid was covering the trap in such a way that the gas molecules could not escape when the vacuum was created. This of course would create a huge damping factor in the oscillation. Therefore two ventilation holes were drilled in the lid. Both holes have a diameter of 400 µm.

3.3.5 Thermalisation

The experiment needs to be executed at very low temperatures. The lowest temperature in the cryostat is reached at the mixing chamber plate and thus our experiment needs to be thermalised to this plate. Thermalisation is done via copper and silver pieces of material. Both metals stay in the metallic state and remain good heat conductors at these low temperatures. In figure 3.4E one of the copper strips can be seen which was used for thermalisation.

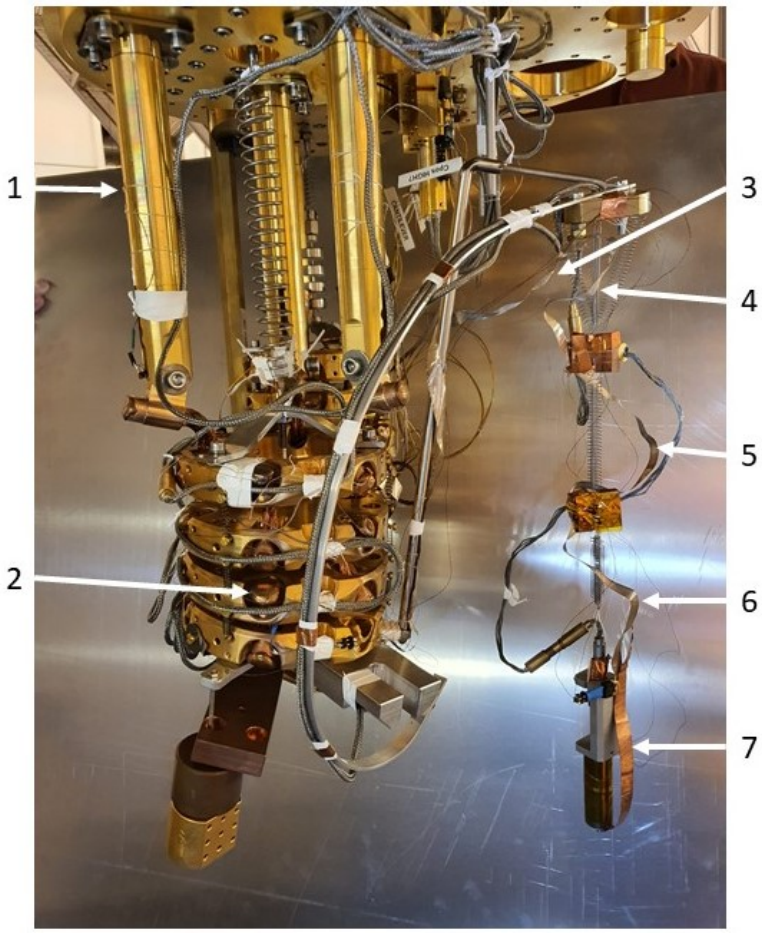

Figure 3.6: *Picture of the experiment. Several stages of the thermalisation are pointed out in the text.*

In figure 3.6 several stages of the thermalisation are pointed out. The mixing chamber plate can be seen at the top, directly attached are three rods (1) which thermally attach the mass spring system to the mixing chamber plate. Copper heat links (2) thermally connect the rods and the masses. From the lower mass onwards there is a flat piece of silver used as a thermal connection, it is via the bendable arm connected to the three masses (3, 4, 5 and 6) and eventually leading to the experiment. The experiment is thermally connected using a flat piece of copper (7).

3.3.6 Etching the Superconductor

The used superconductor is lead. This metal oxidises if it is exposed to water vapour. This is an inevitable process, since the lead traps are made at room pressure. The oxidation causes an insulating layer on the superconductor. This layer can contain electrostatic charges and this may cause the magnet to stick to the surface. To remove this layer the lead is chemically etched.

The etching was done by placing the lead trap in a chemical acid solution of 80 vol% acetic acid and 20 vol% hydrogen peroxide. The acid removes the oxidised material and it also removes a bit of the lead itself. Just a few seconds in the solution is enough to remove the oxidised layer and to not decompose the lead too much. After exposure to the acid solution the lead trap is rinsed in water and dried using a gaseous nitrogen gun.

3.4 Masswheel

As described in the introduction in section 1.2, a rotating wheel with masses attached is used. The used wheel and its casing are shown in the image below. There is an electro motor inside which drives the wheel. All masses are made out of brass and each weigh (2.3672 ± 0.0001) kg.

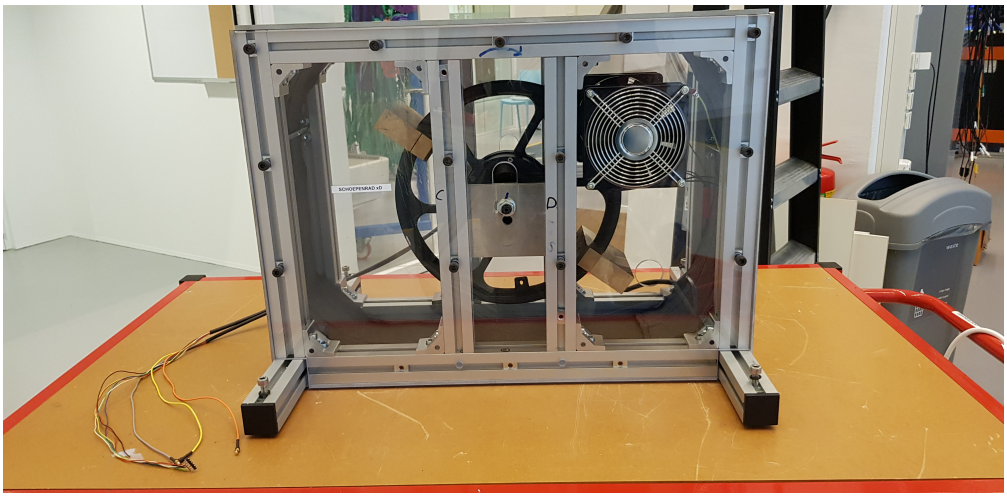

Figure 3.7: *The masswheel with two masses attached.*

The wheel has a diameter of 31 cm. At the top of the wheel there is a laser which is interrupted each time a mass passes. The light is measured by a photo diode, using this signal the frequency of the passing masses can be measured. There is a feedback system such that the wheel can be locked at a desired frequency. The wheel itself can reach up to a frequency of 20 Hz, with two or three masses attached this means a frequency of 40 Hz or 60 Hz respectively for the masses.

The wheel is not perfectly balanced, this causes the wheel and the casing to vibrate. This vibration needs to be isolated from the experiment to not drive the oscillating magnet via mechanical vibrations.

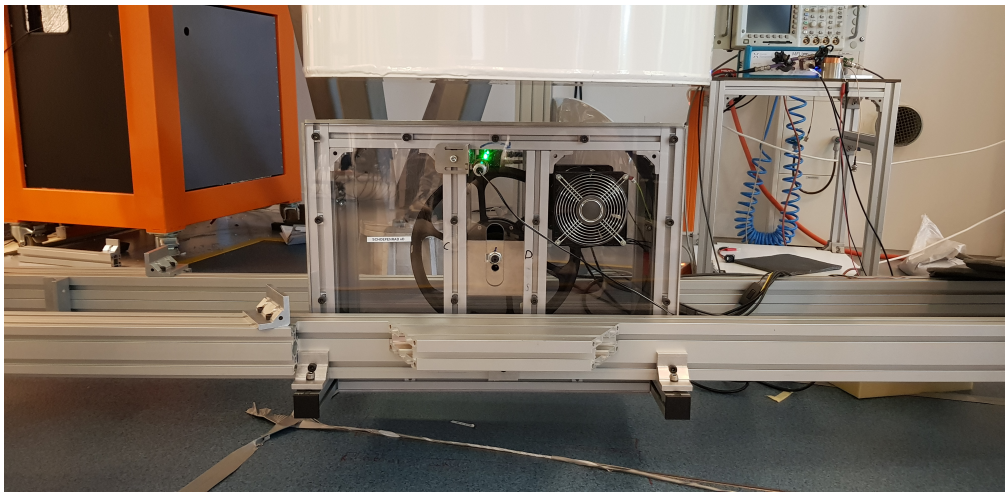

Figure 3.8: *The masswheel on a bridge of MK-profiles just below the cryostat (in white).*

The masswheel is mechanically isolated by a bridge. The oscillation of the bridge is damped by springs. The suspension points of the bridge are on top of dissipative materials which add another damping factor.

With all this vibration isolation between the masswheel and the main floor of the building and the vibration isolation of the cryostat itself there are still some vibrations coupled in. During the experiment several things were tried to damp these vibrations. One of the things that worked out well was the usage of an acoustical damping foam, which comes with a hard cover containing lead. The cover is heavy to act as a dissipative material. This was wrapped directly around the casing of the masswheel, mainly to damp the acoustic vibrations that occur.

The masswheel is right below the cryostat during measurements, so in the space between the cryostat and the floor. The shields of the cryostat and the casing of the masswheel together cause a minimal (vertical) distance of 28 cm between the levitating magnet and the center of mass of one of the masses of the masswheel.

3.5 Measurement Methods

In the introduction two main concepts are introduced to experimentally measure. The first is a levitating magnet and the second is the gravitational interaction between the levitating magnet and a mass outside the cryostat. The methods of how both concepts are experimentally measured are explained below.

3.5.1 Levitation

The concept of a levitating magnet above a superconductor is explained in theory section 2.2. In this subsection it is discussed how it can be confirmed experimentally that the magnet is indeed levitating above the superconductor.

A levitating magnet can be brought in an oscillation via an oscillating magnetic field, then the response of the system can be measured. The N=10 coil was included for this purpose, an oscillating current can be sent through the coil and this will cause the magnet to oscillate. The amplitude of the magnet will of course be largest if this is done at a resonance frequency of the magnet.

The pulse in current through the N=10 coil will create a pulse in magnetic field and after the pulse the magnetic flux of the levitating magnet can be measured. This magnetic flux is measured via the SQUID and if the magnet levitates, the amplitude of the oscillation, and thus the amplitude of the flux, will decrease over time as a response of the system. We refer to this as a magnetic ringdown, the magnet is excited and slowly loses its energy such that the amplitude decreases.

3.5.2 Gravitational Interaction

The measurement of the gravitational interaction between the levitating magnet and the mass outside the cryostat is not straightforward. The difficulty is to exclude all other ways of exciting the magnet. To exclude the mechanical excitation the mechanical movement of the frame of the cryostat can be measured. This movement together with the mechanical damping factor of the system gives the amount of movement at the experiment.

The magnet can be excited by vibrations but also by a magnetic field. Since the masswheel has an electronic motor, it is possible that the motor creates a magnetic field at (a multiple of) the resonance frequency of the magnet. Whether this is a multiple of the resonance frequency or not depends on how the coils inside the motor work, and how many there are.

To be sure that the magnet is excited by gravitational interaction, both the amplitude and the phase shift can be measured. The amplitude depends on the distance with respect to the magnet and the phase shift depends on the angle the wheel has if it is pointing towards the magnet.

The evidence of measuring gravitational interaction is complete if the correct amplitude and the correct phase are measured.

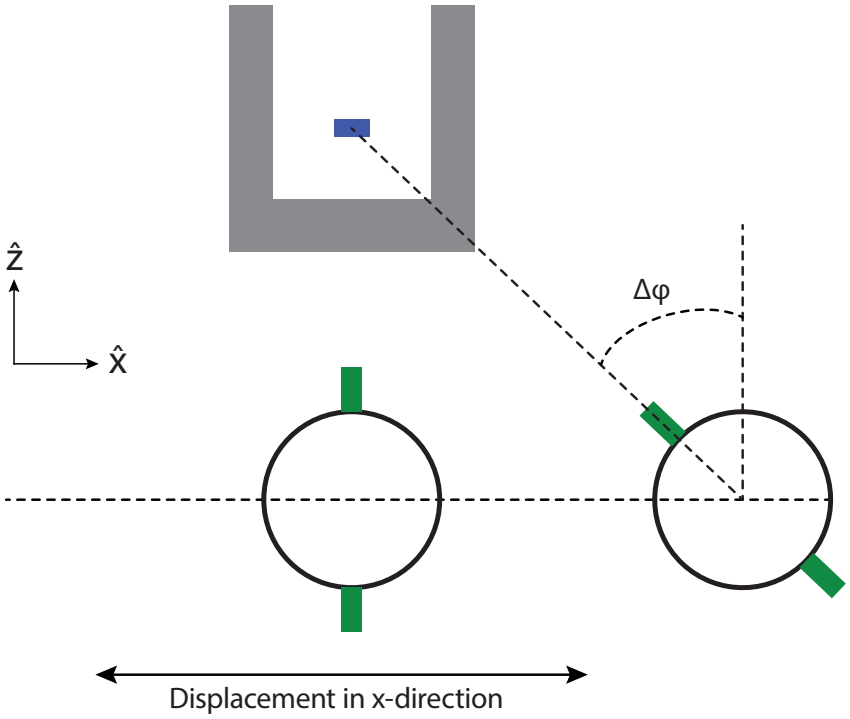

Figure 3.9: *Schematic illustration of the phase shift ($\Delta\varphi$). The superconducting trap is shown in grey, the levitating magnet in blue and the masswheel in black with green masses. The masswheel can move over the indicated direction.*

3.6 Expected Gravitational Interaction

The expected gravitational interaction can be calculated. The masses of both the levitating magnet and the rotating masses are known. Using these together with the minimal distance the maximal gravitational force can be calculated.

$$F_g = \frac{GMm}{r^2} \tag{3.1}$$

$$= 5.8\,\mathrm{fN} \tag{3.2}$$

In this equation G is the gravitational constant ($6.67 \times 10^{-11}\,\mathrm{Nm^2kg^{-2}}$), M is one mass of the masswheel, m is the mass of the levitating magnet and r is the minimal distance between the two centers of mass.

3.6.1 Gravitational Interaction Simulation

The gravitational interaction between the masswheel and the levitating magnet is simulated. This is done for both the case where two masses and where three masses are attached to the masswheel. The amplitude of the force will be larger if two masses are attached, but for three masses the frequency of the masses can be higher. This is a trade off that needs to made, depending on the frequency of the mode. For higher frequencies the vibration isolation also works better.

The simulation uses the masses of the blocks on the masswheel and the mass of the magnet and calculates the gravitational force between the two. The wheel rotates in the xz-plane in this simulation.

In figure 3.10 the gravitational force of one mass rotating for a full cycle is simulated. For the wheel phase equal to 0 and 2π the force in the z-direction has a maximum, for the x-direction there is a maximum and a minimum and the force in the y-direction is invariant for the rotation of the wheel. The wheel is rotating in the xz-plane, this causes the asymmetry in the x-direction and also that the force in the y-direction is invariant for the rotation of the wheel.

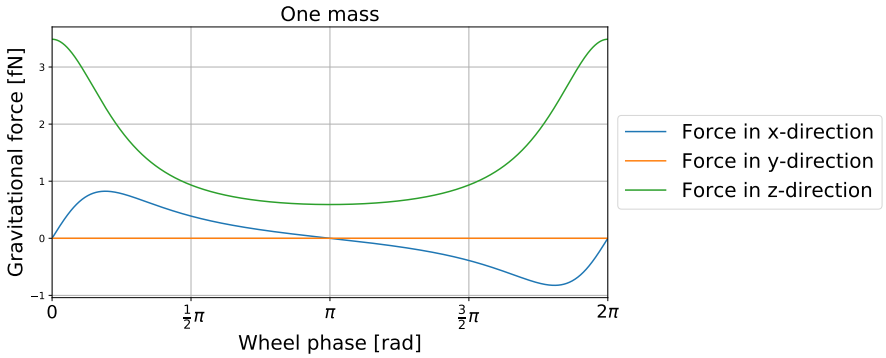

Figure 3.10: *Gravitational force from one block on the magnet simulated.*

In reality it is impossible to have a masswheel with one rotating mass, the center of mass of the wheel would not be at the axis of the wheel and this would create lots of vibrations and eventually cause the wheel to break. With two or three (or more) masses attached, this problem can be solved using rotational symmetries. Therefore the gravitational force of two and three masses are simulated in figure 3.11.

In this figure it can be seen that the number of maxima in the z-direction is equal to the number of masses. This is due to the fact that if a mass is at the top of the masswheel the distance in the z-direction will be shortest between the mass and the magnet. This creates a maximum in the gravitational force.

By comparing the gravitational force in the z-direction between two masses and three masses in figure 3.11, it can be seen that the magnitude is highest in the case of three masses. This is because the total mass of the masswheel is higher and thus the total gravitational force is larger. What also can be seen is that the difference in gravitational force for the case of two masses between a minimum and a maximum is larger than in the

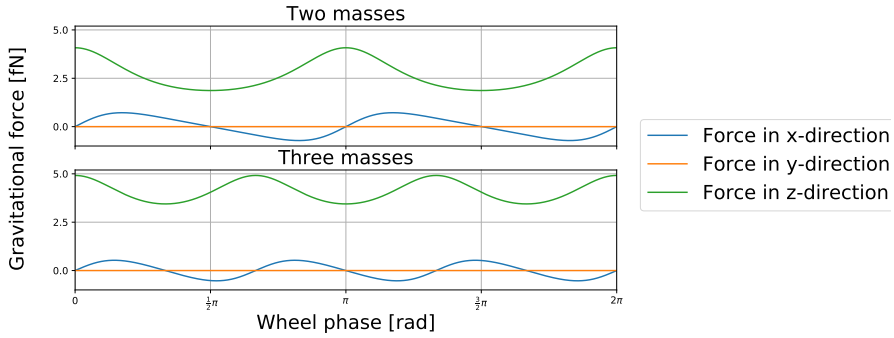

Figure 3.11: *Gravitational force simulated between the magnet and two (upper) or three (lower) blocks attached to the masswheel.*

case of three masses. This difference will eventually create the gravitational interaction force, and this force will thus be larger for fewer masses.

In the x-direction there is always a minimum and a maximum around the z maximum. In the x-direction the magnet is attracted firstly to a mass in the negative x-direction and after passing beneath the magnet the magnet is attracted in the positive x-direction. The force in the y-direction is still invariant under rotation of the wheel since it is symmetric in that direction.

The wheel can now be shifted in the x-, y- and z-direction. This is done by changing the position of the wheel in the simulation. Firstly this is done for the x-direction. In figure 3.12 this is shown.

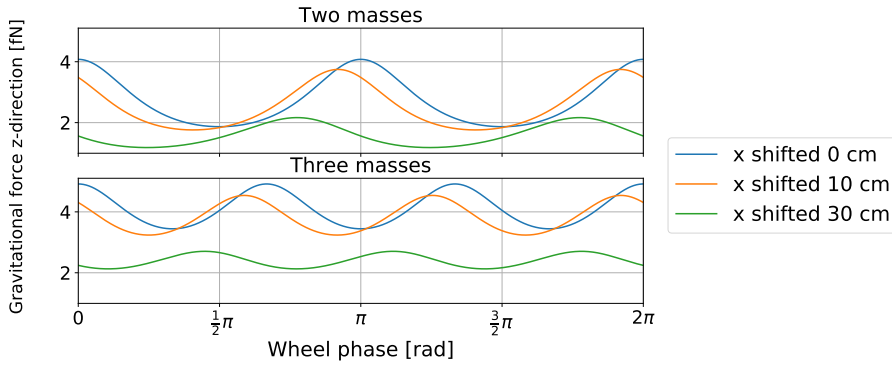

Figure 3.12: *Gravitational force in the z-direction simulated between the magnet and different x-positions of the wheel. Upper figure has two masses attached to the masswheel and the lower figure three masses attached.*

For the shift in the x-direction it can be clearly seen that the amplitude of the force decreases for an increasing distance. The maximum in the force also shifts away. This is called the phase shift, as illustrated in figure 3.9.

Secondly the same can be done in the y-direction, see figure 3.13.

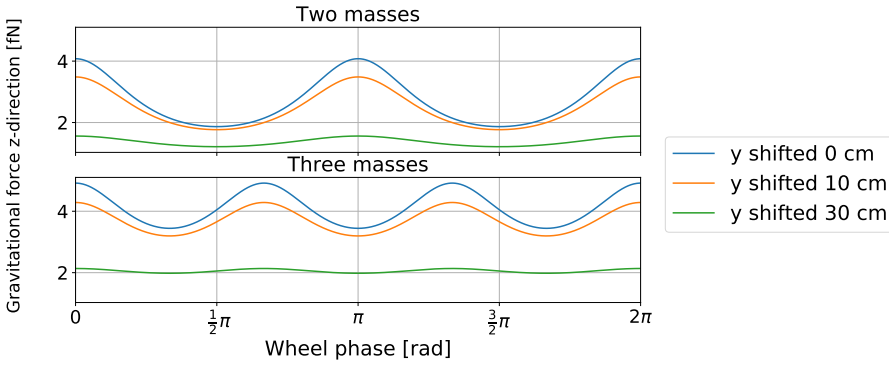

Figure 3.13: *Gravitational force in the z-direction simulated between the magnet and different y-positions of the wheel. Upper figure has two masses attached to the masswheel and the lower figure three masses attached.*

The shift in the y-direction also causes the amplitude to decrease, but it does not create a phase shift. This is because the wheel rotates in the xz-plane and the force thus doesn't create a component which causes the phase to shift.

Thirdly the z-direction is changed, depicted in figure 3.14.

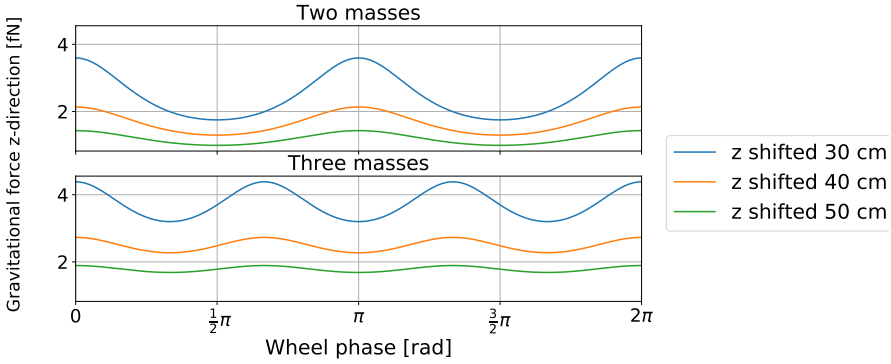

Figure 3.14: *Gravitational force in the z-direction simulated between the magnet and different z-positions of the wheel. Upper figure has two masses attached to the masswheel and the lower figure three masses attached.*

The shift in the z-direction causes the wheel to be lower beneath the magnet. The further away the wheel the smaller the force and the lower the amplitude of the force. There is no phase shift introduced because only the z-coordinate is changed.

In all figures so far it can be seen that the amplitude of the simulation for two masses is larger than the amplitude for three masses. This is because the angle between the masses is larger for two masses and thus the next passing mass is further away for a wheel with two masses.

These figures can be produced not only for the force of the z-mode, but also for the force of the x- and y-mode. These figures are skipped in this thesis but conceptually they are the same.

For the next step the Fourier transform of the force can be taken. This is done for a range of positions, for the x- and y-direction from −50 cm to 50 cm and for the z-direction from 25 cm to 50 cm. With this Fourier transform the amplitude and phase shift of the force of the x-, y- and z-mode can be calculated.

In figure 3.15 the amplitude in the x-mode (upper figure), y-mode (middle figure) and the z-mode (lower figure) can be seen. The different colors represent a shift in a different direction. The solid lines are for two masses on the wheel and the dashed lines are for three masses on the wheel.

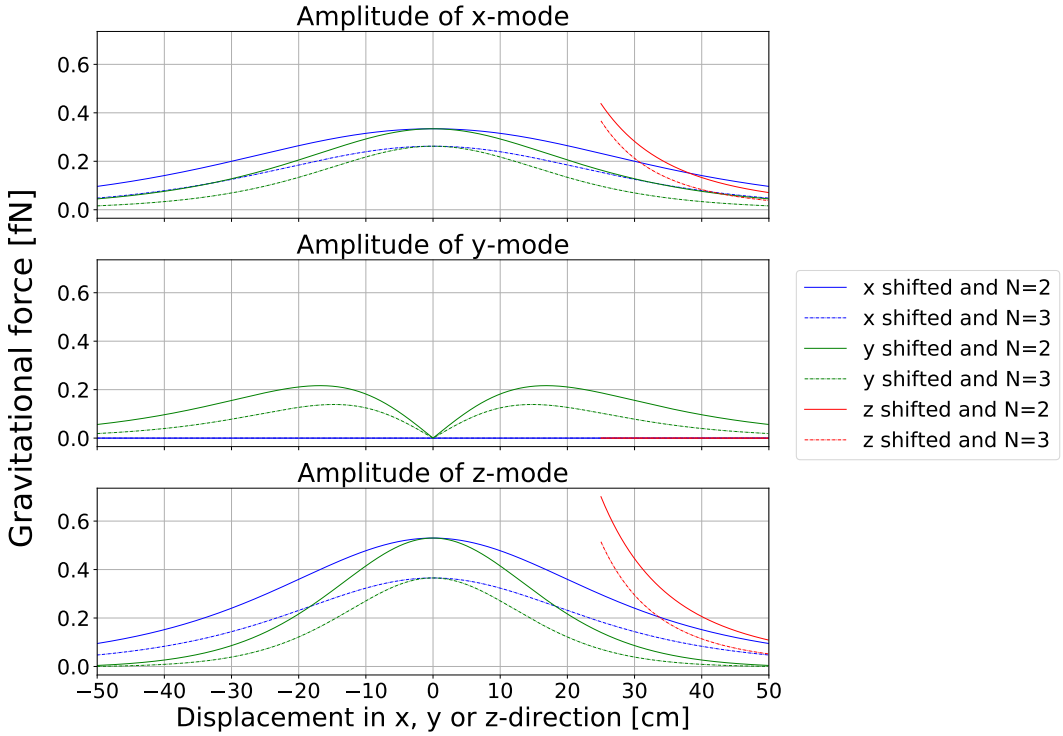

Figure 3.15: *The amplitude of the gravitational force is simulated. The wheel turns a full rotation in this simulation at every position. The upper figure is the force amplitude for the x-mode, the middle figure for the y-mode and the lower figure for the z-mode. In every figure the masswheel is shifted from* −50 cm *to* 50 cm *in the x- and y-direction and from* 25 cm *to* 50 cm *in the z-direction. In the z-direction the wheel cannot come closer to the magnet and can not be lowered more than these values. The different colors show the different displacement directions. The solid lines are for a masswheel with two masses (N=2) attached and the dashed lines for three masses (N=3) attached.*

In this figure it can be seen that the forces in all directions are symmetric. For the y-mode the shift in x and z are all equal to zero, again because these don't exert a force due to the rotational plane of the wheel.

Next the phase of the forces in all three dimensions are plotted in figure 3.16.

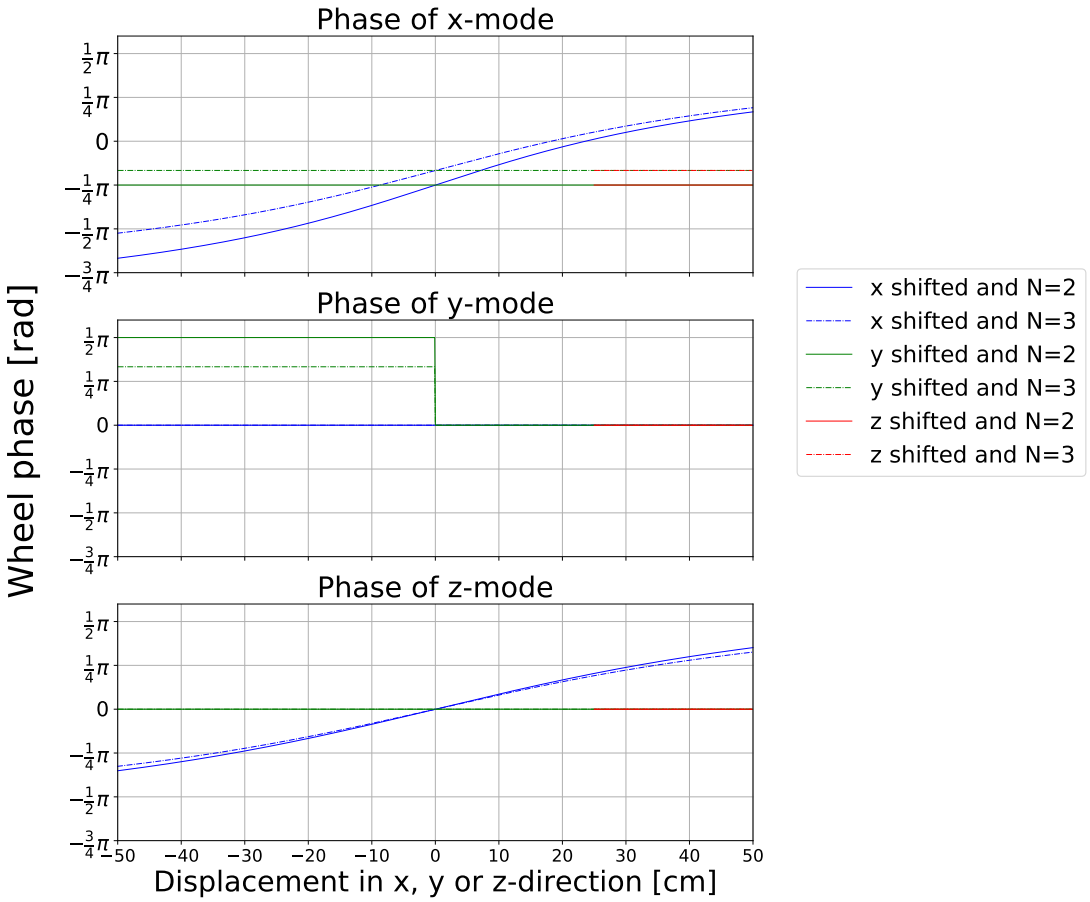

Figure 3.16: *The phase of the gravitational force is simulated. The wheel turns a full rotation in this simulation at every position. The upper figure is the force phase for the x-mode, the middle figure for the y-mode and the lower figure for the z-mode. In every figure the masswheel is shifted from* $-50\,\text{cm}$ *to* $50\,\text{cm}$ *in the x- and y-direction and from* $25\,\text{cm}$ *to* $50\,\text{cm}$ *in the z-direction. The different colors show the different displacement directions. The solid lines are for a masswheel with two masses (N=2) attached and the dashed lines for three masses (N=3) attached.*

For the phases of the x-mode only the shift in x is not constant. The other shifts only cause a constant phase shift, which is not equal to zero. The force in the y-direction has a step of $\pi/2$ for two masses, and $\pi/3$ for three masses, if the y-displacement passes zero. This means that there is negative phase shift for a negative y-displacement and a positive phase shift for a positive y-displacement. In the z-direction of the force again only the shift in x creates a phase shift which is not constant.

3.7 Gravity by the Moon and the Tides

The levitating magnet also experiences a gravitational interaction with the moon. If the moon is straight above or below the magnet it will be vertically lifted. Furthermore the magnet is located only 6.2 km away from the North Sea as the crow flies. The tides of the North Sea will also change the position of the magnet within the superconducting trap.

3.7.1 Gravity by the Moon

The magnet and the moon are constantly having gravitational interaction. The location of the moon with respect to the superconducting trap determines the direction of the interaction. If the moon is right above or below the magnet the magnet will have a slightly higher levitation height. The mass of the moon is known to be $M_{\text{Moon}} = 0.012 M_{\text{Earth}}$ with M_{Moon} the mass of the moon and M_{Earth} the mass of the earth. The distances compare as: $r_{\text{Moon}} \simeq 60 r_{\text{Earth}}$ where r_{Moon} is the distance between the moon and the magnet and r_{Earth} is the distance between earth's center of mass and the magnet. With these two values the gravitational acceleration due to the moon can be calculated: $g_{\text{Moon}} = g_{\text{Earth}} \frac{M_{\text{Moon}}}{M_{\text{Earth}}} \left(\frac{r_{\text{Earth}}}{r_{\text{Moon}}}\right)^2 = 32.7\,\mu\text{m/s}^2$. In this expression g_{Moon} is the gravitational acceleration due to the moon. The change in levitation height due to the moon can be calculated as: $\Delta z_{0,\text{Moon}} = z_0 \cdot \left(\frac{g_{\text{Earth}}}{g_{\text{Earth}} - g_{\text{Moon}}}\right)^{1/4} - z_0 = 1.7\,\text{nm}$. This is in the order of the oscillation amplitude of the magnet.

3.7.2 Gravity by the Tides

The part of the North Sea closest to the magnet will have the largest contribution to the lateral shift due to the tides. Therefore not the whole North Sea is taken into account. Measured from Katwijk aan Zee, which is where the sea is closest to Leiden, it is roughly 200 km to the coast of Great Britain in the west and 100 km to Den Helder to the north. The same distance is taken in southerly direction. In Katwijk the difference in the water height is 1.6 m between high and low tide. This gives a volume of water in difference between high and low tide of $64 \times 10^9\,\text{m}^3$. Using a density of water of one kg per litre, this is equal to a mass difference of 64×10^{12} kg. The center of mass is in the middle of this part of the sea 100 km from the coast plus the distance from the magnet to the coast (6.2 km). This results in a gravitational acceleration of $g_{\text{Tides}} = G \frac{m_{\text{water}}}{r_{\text{water}}} = 0.38\,\mu\text{m/s}^2$.

The result of this calculation strongly depends on how much water is taken into account. Over the whole surface the water height difference will not be the same. This calculation however gives an indication of the order of magnitude of this gravitational acceleration.

Since the sea water is in the lateral plane of the magnet a change in levitation height will not occur. A change in the lateral position will occur due to the tides. The exact expression for the lateral modes is not known and therefore this shift cannot be calculated.

Chapter 4

Results

The signal of the magnet inside the cooled trap is characterised, to find the resonances of the particle. The measurements start by calculating a spectrum using a fast Fourier transform (FFT). This is done using the SQUID data, which is a signal in the time domain.

When the spectrum is known the eigenfrequencies can be searched. The spectrum is filled with all kinds of resonance peaks, for example the pulse tube and its higher harmonics are seen as lots of peaks in the spectrum. Furthermore not only vibrations create peaks in the spectrum, but external electromagnetic signals will also contribute. The AC 50 Hz from the power lines and its harmonics for example are measured during every run of the experiment, despite measures to avoid such signals coupling in

When the peaks which are explainable by external sources are filtered out, the leftover peaks can be tried to drive vibrationally or magnetically. We believe magnetic drive gives the best guarantee that a resonance peak is indeed due to the particle moving rather than due to a moving wire. This is done according to the method discussed in 3.5.1.

4.1 Magnetic Ringdown

Usually it takes several tries at different frequencies to magnetically excite the magnet. Also, it may take some effort to keep the SQUID locked while driving magnetically. In figure 4.1 an example of several attempts is shown. On the vertical axis of the upper figure the amplitude is given in volts on a logarithmic scale, on the horizontal axis the time (date and hour) is given on a linear scale. The lower figure shows the phase of the signal on the same timescale. The part between the two dotted red lines is a magnetically driven ringdown. The frequency of the used lock-in amplifier changed a couple of times between the beginning and end of this graph. Between the two dotted red lines the lock-in frequency was continuously 52.505 Hz.

In the figure it can be seen that the ringdown actually started a little earlier than the first dotted red line. The peaks at the start of the ringdown indicate some adjustments

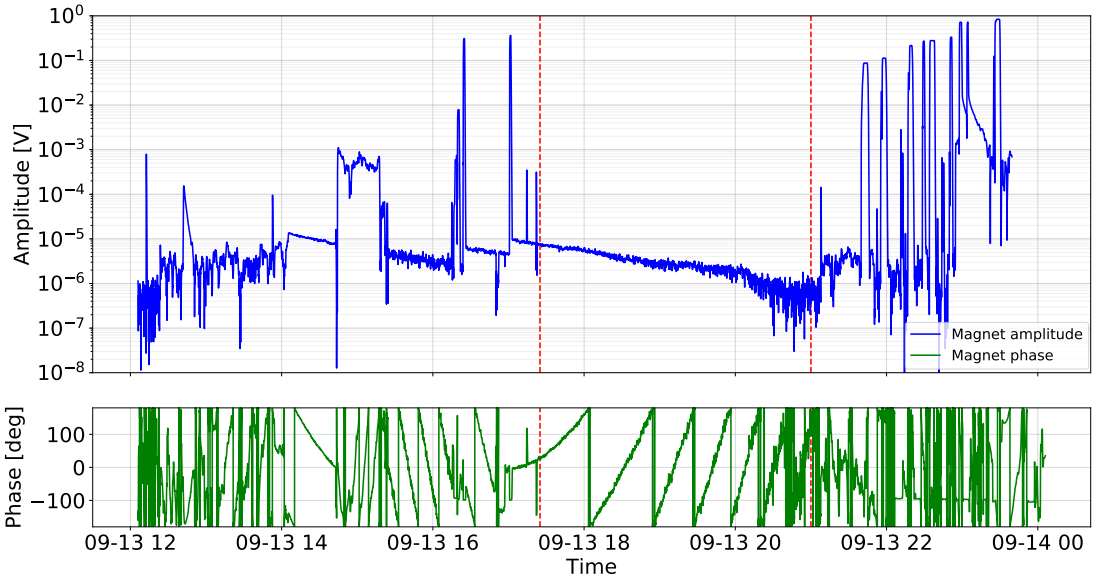

Figure 4.1: *The SQUID signal measured via the lock-in, the lock-in frequency was changed several times during this timespan. The upper figure shows the amplitude in volts on a logarithmic scale and the lower figure the phase in degrees on a linear scale. The measurement lasts 12 hours.*

in the settings or some short magnetic flux pulses. Therefore the cut out ringdown is started just after these peaks.

Now the part between the two dotted red lines is cut out, this is the used ringdown for further data analysis. In figure 4.2 this data is shown. Now the amplitude axis is both given in volts and in picometers, using the flux position conversion (section 4.3).

Looking at figure 4.2, three things stand out. The first is the noise in the amplitude. The larger the amplitude, the smaller the relative noise. The second is that there is a phase shift with respect to the lock-in, which is not constant. The slope of the phase is the difference between the resonator frequency and the lock-in frequency. The slope of the phase shift becomes steeper as the amplitude becomes smaller. The third is the noise in the phase, this noise is smaller for larger amplitudes.

The amplitude is used to fit an exponential function of the form:

$$f(t) = Ae^{-t/\tau} \tag{4.1}$$

Where A is the amplitude, t is the time and τ is the damping time. The python routine uses a least-squares method to fit this function and it is shown in yellow in the figure. The results are for the amplitude (204.0±0.9) µV, or (90.0±0.4) nm, and for the damping time (5823±7) s.

Now the Q factor can be calculated as:

$$Q = \frac{1}{2}\omega_0\tau = 960 \times 10^3$$

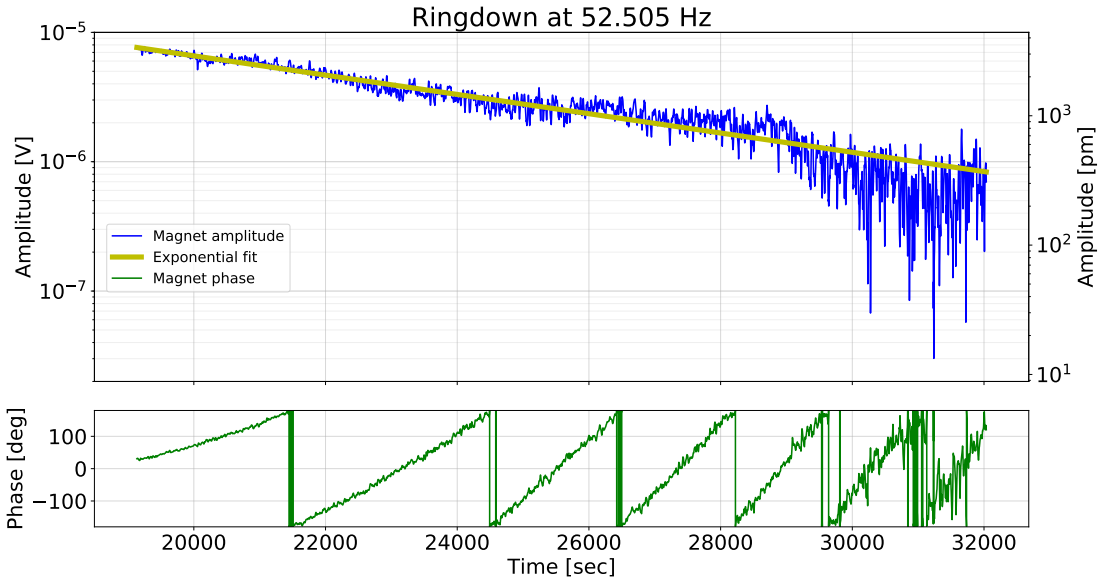

Figure 4.2: *The SQUID signal measured via the lock-in of a magnetic ringdown. The amplitude is given in volts and in picometers (using section 4.3) on a logarithmic scale, the phase is given in degrees on a linear scale. The yellow line is an exponential fit to the data in blue.*

Where ω_0 is taken equal to the lock-in frequency. The frequency is different and does shift during the ringdown, but this is an insignificant change of $10 - 20$ ppm compared to the uncertainty in the damping time.

4.2 Energy Coupling

The energy coupling can be determined by driving the magnet magnetically. The amplitude and phase of the magnet are measured before, during and after driving the magnet. These measurements are used to calculate the energy coupling. This measurement takes place at 52.505 Hz.

Firstly, the amplitude and phase are plotted from the start of the measurement till the end of the measurement. At the start, the lock-in frequency is adjusted. When the lock-in does not have the right frequency, the phase jumps from +180° to -180° or vice versa, as happened in figure 4.3 at the beginning.

In figure 4.3 vertical red dotted lines are visible, these are cutting lines of the data. The first part between the two cutting lines is the data used before the drive (orange), the next part between the cutting lines is during the drive (blue) and the last part is after the drive (green). From this figure it can be concluded that this drive was actually a drive up, since the amplitude before drive is lower than the amplitude after drive. The drive was performed when the phase was around zero degrees, because the drive needs to be 90° out of phase with respect to the magnet.

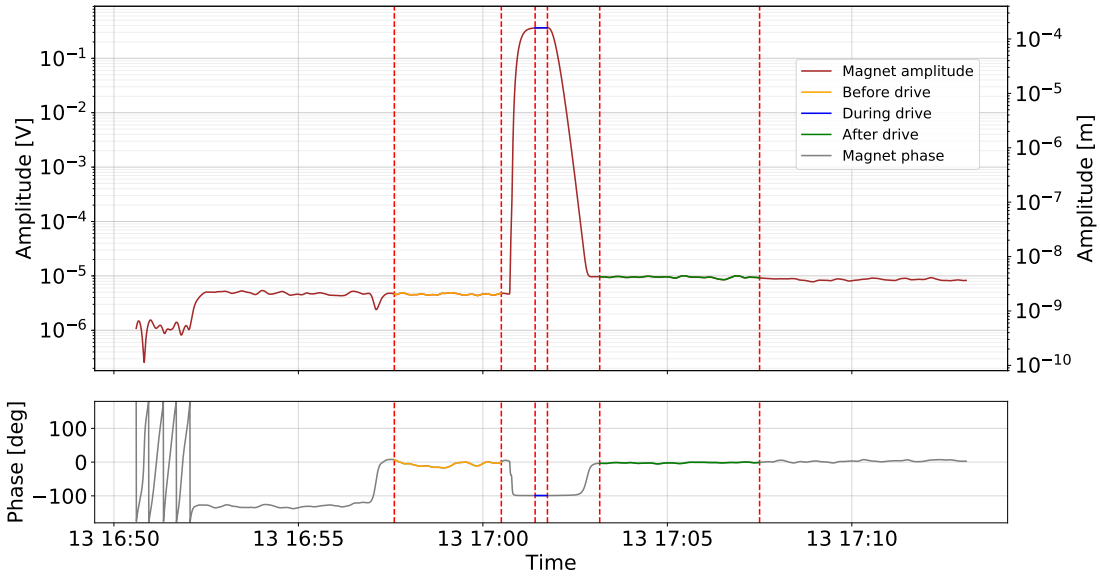

Figure 4.3: *The data used to determine the energy coupling. The vertical dotted red lines are the cutting lines. The first part between cutting lines is before drive, the second part is during drive and the last part is after drive. The amplitude is given in volts and in meters (using section 4.3).*

The three parts are now plotted in the complex plane. The amplitude and phase of each point are used to create this data point. The data is plotted in the complex plane in figure 4.4. During drive the amplitude is roughly five orders of magnitude larger than before and after the drive. In the upper half of figure 4.4, only the data during drive can be distinguished for this reason. The lower half of figure 4.4 shows a zoomed in view on the data before and after drive. The two red dotted lines in the lower figure show the angle between the drive vector and the vector showing the difference between before and after drive.

In the lower half of figure 4.4 the vertical and horizontal axes are chosen the same such that the angles in this plot are correct. This is not the case in the upper half of the figure. The angle between the vectors during drive and the difference between before and after drive is: $-99.18° - (-2.13° + 6.89°) = -103.94°$. This is not exactly the same as the theoretical 90°, it is off by 15%. A future more careful and repeated measurement would be needed to determine whether this is within the measurement error.

The energy coupling can now be calculated using the energy coupling theory (section 2.6) as follows:

$$\beta^2 = \frac{\Delta\Phi_{\text{particle motion}}}{\Phi_{\text{drive}}\ Q} = \frac{\Delta V_{\text{particle motion}}}{V_{\text{drive}}\ Q} \tag{4.2}$$

$$= \frac{9.47 \times 10^{-6} - 4.61 \times 10^{-6}}{363.20 \times 10^{-3} \cdot 960 \times 10^{3}} \tag{4.3}$$

$$= 1.40 \times 10^{-11} \tag{4.4}$$

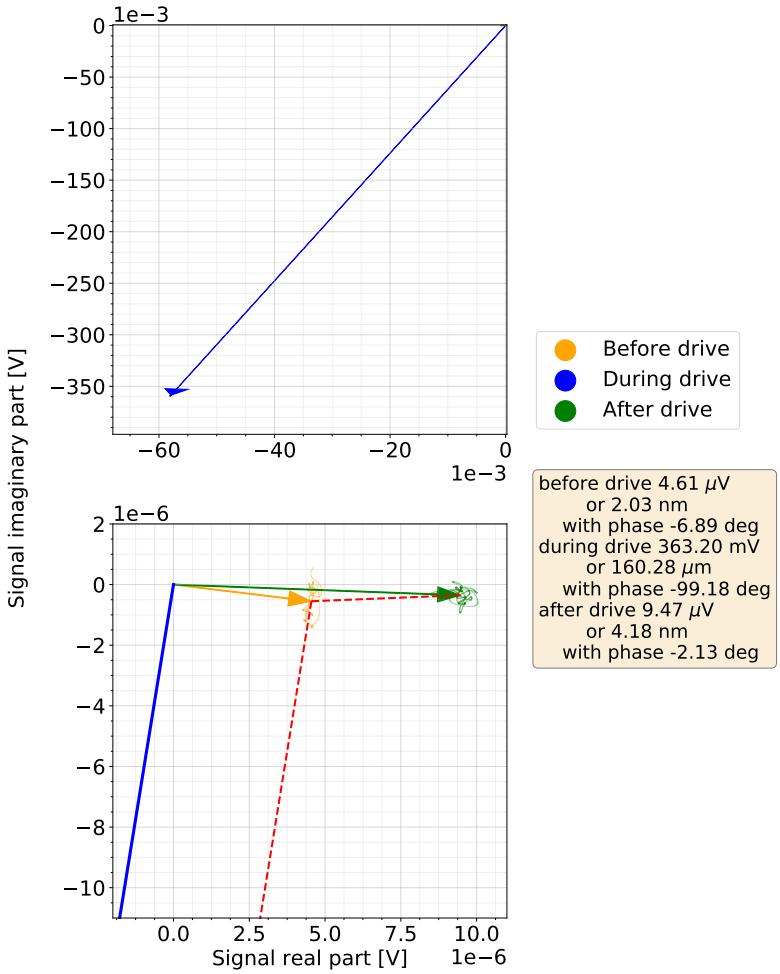

Figure 4.4: *The three parts of the signal plotted in the complex plane. The upper half of the figure shows all of the data and the lower half zooms in on the data before and after the drive. In the lower figure the dotted red lines are to show the angle between the drive and the result of the drive. Below the legend in the figure the amplitude and the phase of all vectors are shown.*

The magnetic flux is proportional to the SQUID voltage, therefore the SQUID voltage can directly be used to calculate the energy coupling. The same method is used for every mode to calculate their energy coupling independently.

4.3 Flux Position Conversion

The derived flux position conversion as in theory section 2.6.1 can now be derived.

All values are known, and the displacement as a function of measurement voltage is: $\frac{dx}{dU} = -441\,\mu\mathrm{m/V}$. This values is already used in some of the previous graphs in this chapter to convert the amplitude from volts to meters.

4.4 Vibration Isolation

The mechanical vibration isolation is measured in two different ways. The first method uses a mechanical actuator to create vibrations in the frame of the cryostat. The second method uses the masswheel as a source of vibrations.

4.4.1 Actuator

A mechanical actuator is used to create vibrations in the frame of the cryostat. This was done for several hours, the data is plotted in figure 4.5. The data between the two vertical dotted red lines is used in the next steps. The figure shows the amplitude and phase of both the magnet and the Güralp, the Güralp is the brand of the vibration measurement device. The amplitude is given in nanometres and the phase in degrees.

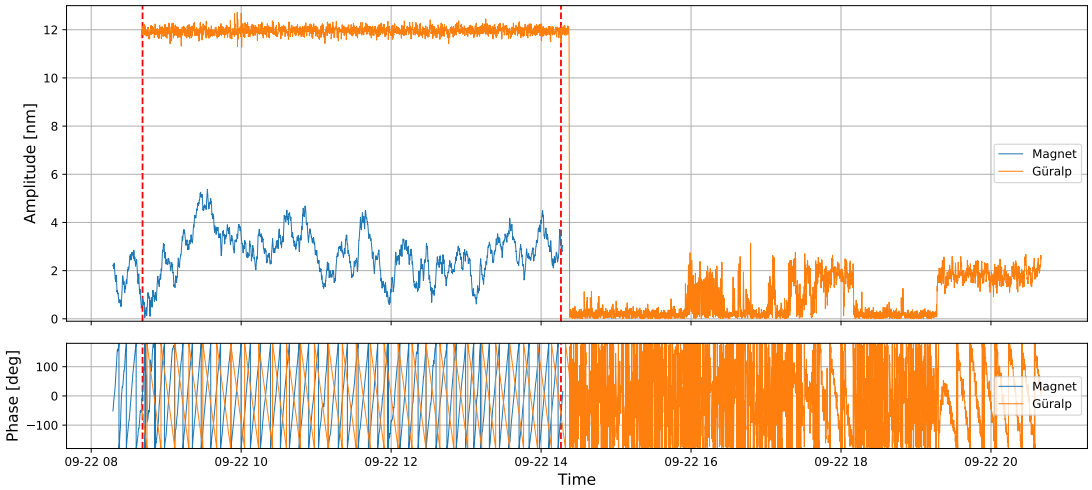

Figure 4.5: *The lock-in data used for calculating the vibration isolation. The two vertical dotted red lines indicate the cutting lines of the used data. The measurement lasts 12 hours.*

A Fourier transform of this data is taken using a fast Fourier transform. These measurements were performed using a lock-in, this results in the fact that a frequency of zero corresponds to a frequency shift of zero with respect to the lock-in frequency. The Fourier transform is plotted in figure 4.6.

This plot contains the amplitude in m^2/Hz of the Fourier transform. The spectrum of a harmonic oscillator has a Lorentzian around the resonance peak. This Lorentzian fit is performed using Python with a least-squares method. The full width half maximum (FWHM) of this Lorentzian is equal to f/Q, according to section 2.1.2. The value for the FWHM is 58.3 µHz. The lock-in is at a frequency of 54.1405 Hz, so the Q factor is 929×10^3.

The damping can now be calculated using this spectrum. The damping is calculated as the ratio between the movement of the frame and the movement of the trap in decibels.

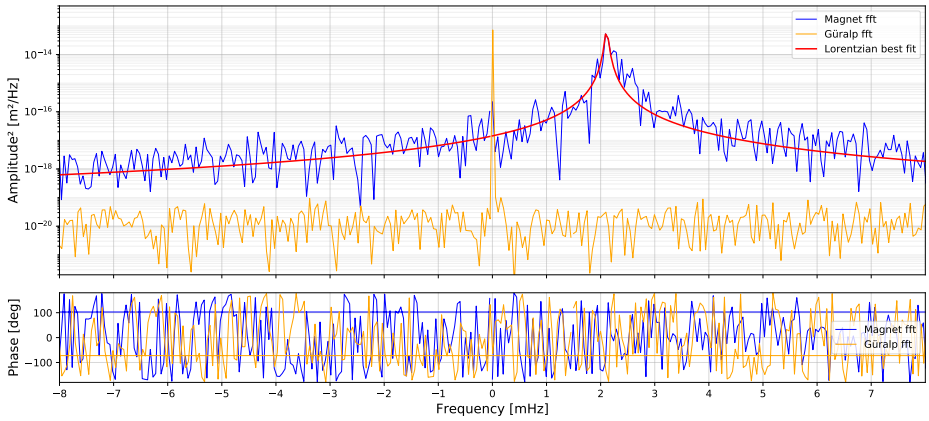

Figure 4.6: *The spectrum of the vibration detector (Güralp) and the magnet using a fast Fourier transform. A Lorentzian function is fitted to the spectrum of the magnet. The amplitude is plotted squared in* m^2/Hz *and the frequency is relative to the lock-in frequency. This means that a frequency of zero in the graph corresponds to a frequency of* 54.1405 Hz *in reality.*

Using the transfer function between the trap and the magnet, the spectrum of the trap can be calculated from the spectrum of the magnet. The damping is calculated via:

$$\text{Damping} = 20\ {}^{10}\log\left(\frac{\text{Güralp movement}}{\text{Trap movement}}\right) \tag{4.5}$$

The values of movement are taken at the frequency of the actuator, in figure 4.7 this is at zero Hertz, where the dots are. Using these values the damping is calculated to be 111 dB.

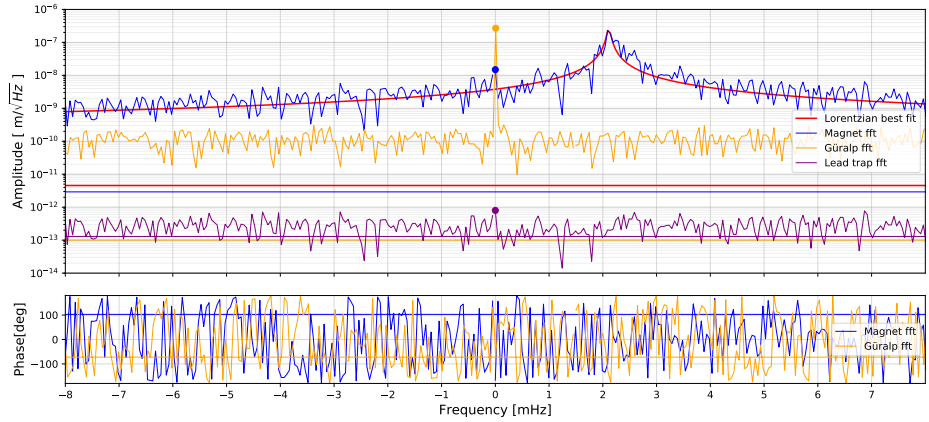

Figure 4.7: *The spectrum of the vibration detector (Güralp) and the levitating magnet is plotted using a fast Fourier transform. The amplitude is plotted in* $m/\sqrt{Hz}$ *on a logarithmic scale. The spectrum of the lead trap is calculated using the spectrum of the magnet and the transfer function between the trap and the magnet. The frequency in the graph is relative to the lock-in frequency, a frequency of zero in the graph corresponds to* 54.1405 Hz *in reality.*

4.4.2 Rotating Masswheel

The masswheel can also be used as a source of vibrations. By comparing the spectrum of the lead trap and the Güralp the vibration isolation can be calculated.

The masswheel was turned on at a frequency just below the eigenfrequency of the magnet. Both the SQUID and the Güralp were measured using a lock-in amplifier. The measured signal is shown in figure 4.8, both the amplitude and the phase are depicted. Two dotted vertical red lines indicate the cutting lines of the used data.

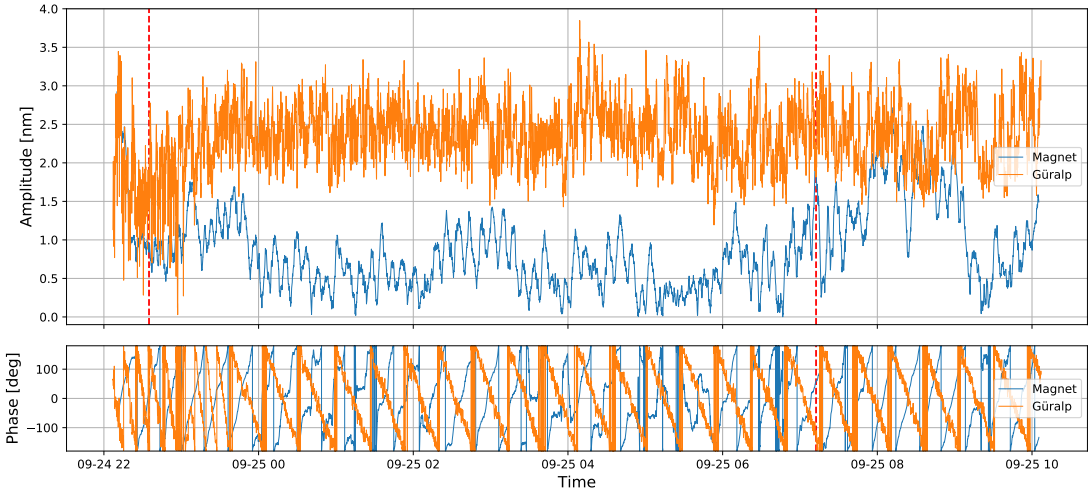

Figure 4.8: *The amplitude and the phase of the magnet and the Güralp are plotted. The masswheel is used as a source of vibrations. The measurement lasts 12 hours.*

Now a fast Fourier transform (FFT) can be performed of the data between the cutting lines. Since the masswheel contains a laser which is interrupted each time a block passes the FFT can also be taken from the laser signal. The amplitude of the FFT is squared and a Lorentzian is fitted on the spectrum of the magnet. The amplitude of the laser has arbitrary units since this is just the voltage of the detector of the laser light. This is all depicted in figure 4.9.

Again a Q factor can be determined using this Lorentzian fit, using the definition described in section 2.1.2. The full width half maximum (FWHM) value is 102.1 µHz, the frequency of the lock-in was 54.1425 Hz. This results in a Q factor of 530×10^3.

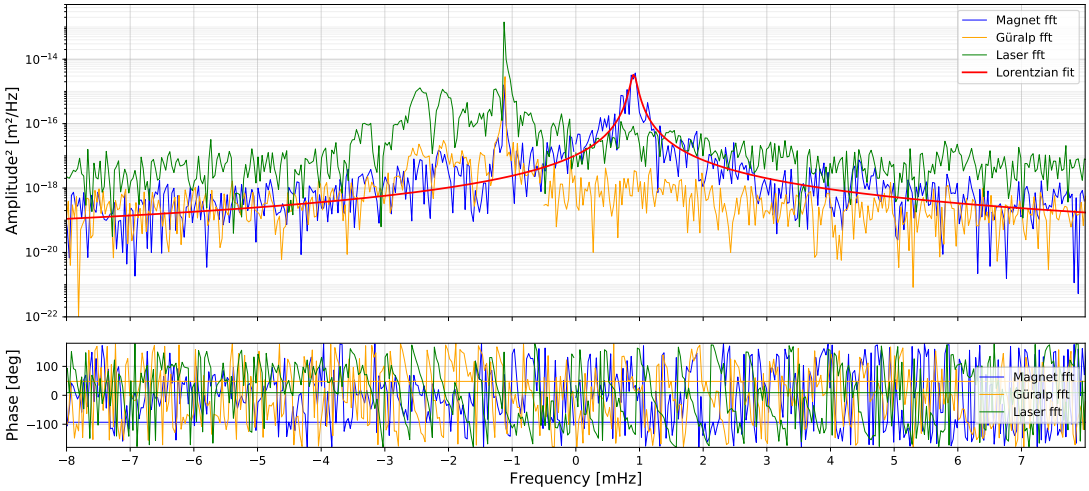

Figure 4.9: *The spectrum of the magnet and the Güralp obtained using a fast Fourier transform. A Lorentzian is fitted to the spectrum of the magnet to be able to determine the Q factor. The spectrum amplitude of the laser has arbitrary units. The frequency in the graph is relative to the lock-in frequency, a frequency of zero in the graph corresponds to a frequency of* 54.1425 Hz *in reality.*

The next step is to calculate the damping. This is done using the method in equation 4.5. This is done at the frequency of the masswheel, this is where the dots are in figure 4.10. This results in a damping of 92 dB.

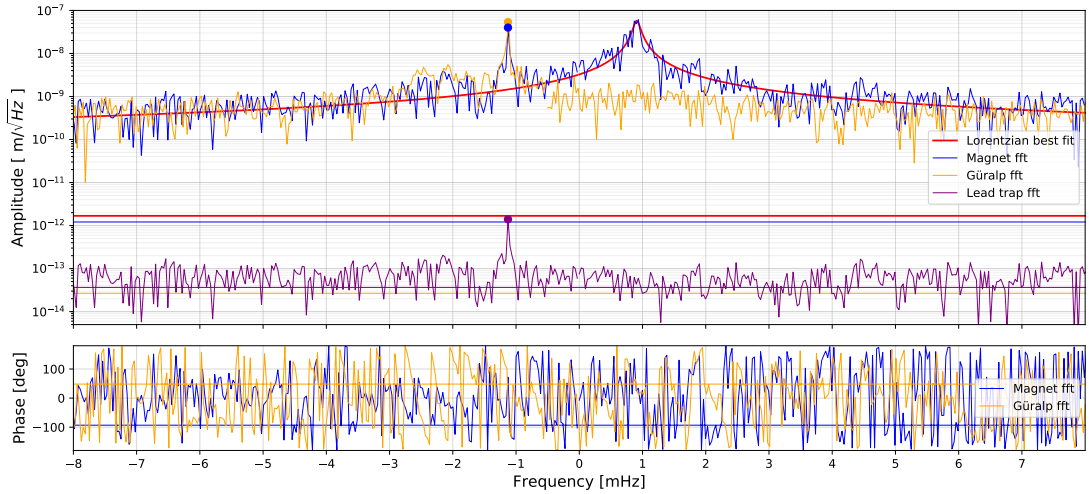

Figure 4.10: *The spectrum of the magnet, Güralp and the lead trap. The spectrum of the lead trap is determined by the spectrum of the magnet and the transfer function between the trap and the magnet. The dots indicate the peak in the spectrum of the masswheel and these values are used to calculate the damping. The frequency in the graph is relative to the lock-in frequency, a frequency of zero in the graph corresponds to a frequency of* 54.1425 Hz *in reality.*

4.5 Gravitational Interaction

As described in method sections 3.5.2 and 3.6 the amplitude and phase of the gravitational force are measured. This principle is based on moving the masswheel around below the cryostat in a particular direction and using this to determine which mode is driven. Therefore the measured points are plotted in all three plots for the amplitude and for the phase. The measured data used three masses attached to the the wheel (N=3). Then by comparing these results, one would like to determine which mode was driven.

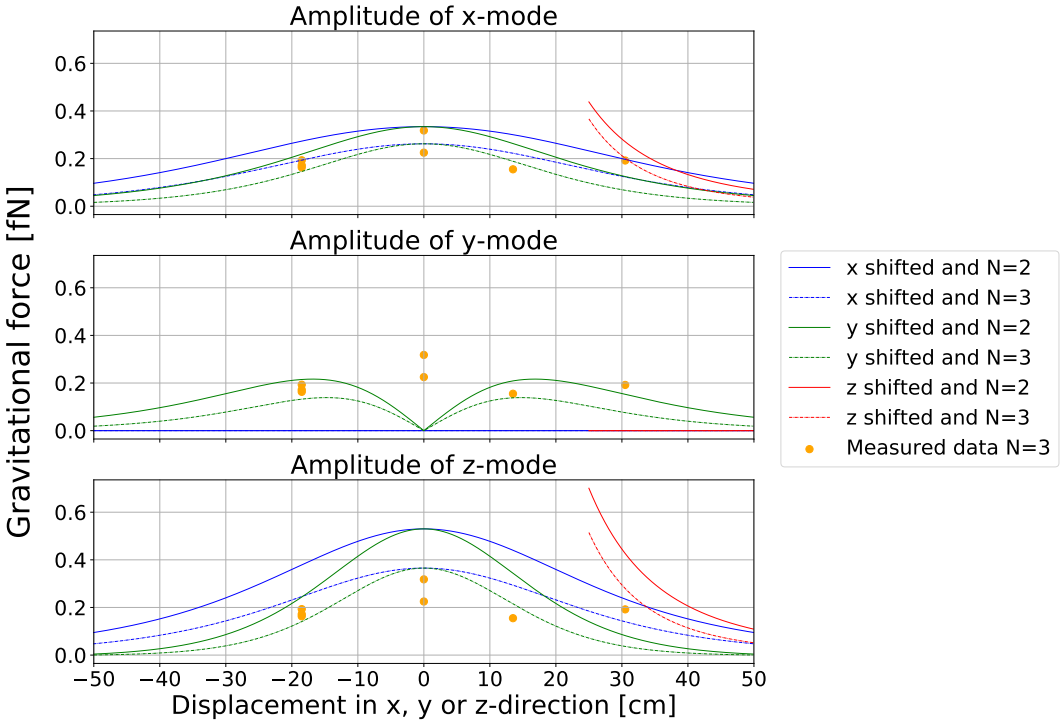

Figure 4.11: *The expected and the measured amplitude of the gravitational force are shown. The three graphs show the different x-, y-, and z-modes. The different colors show the different displacement directions. The solid lines show the expected values for a masswheel with two masses (N=2) attached and the dashed lines the expected values for a masswheel with three masses (N=3) attached. The measured points are plotted in all three lateral directions (x, y and z) because it is unknown which mode corresponds to this frequency. The measured data used three masses on the wheel (N=3).*

Figure 4.11 shows the expected and the measured amplitude of the gravitational force. In this plot the same measured amplitude at different locations are shown in each graph, since we do not know which mode (a lateral x-, y- or z-mode or a rotational mode) this frequency corresponds to.

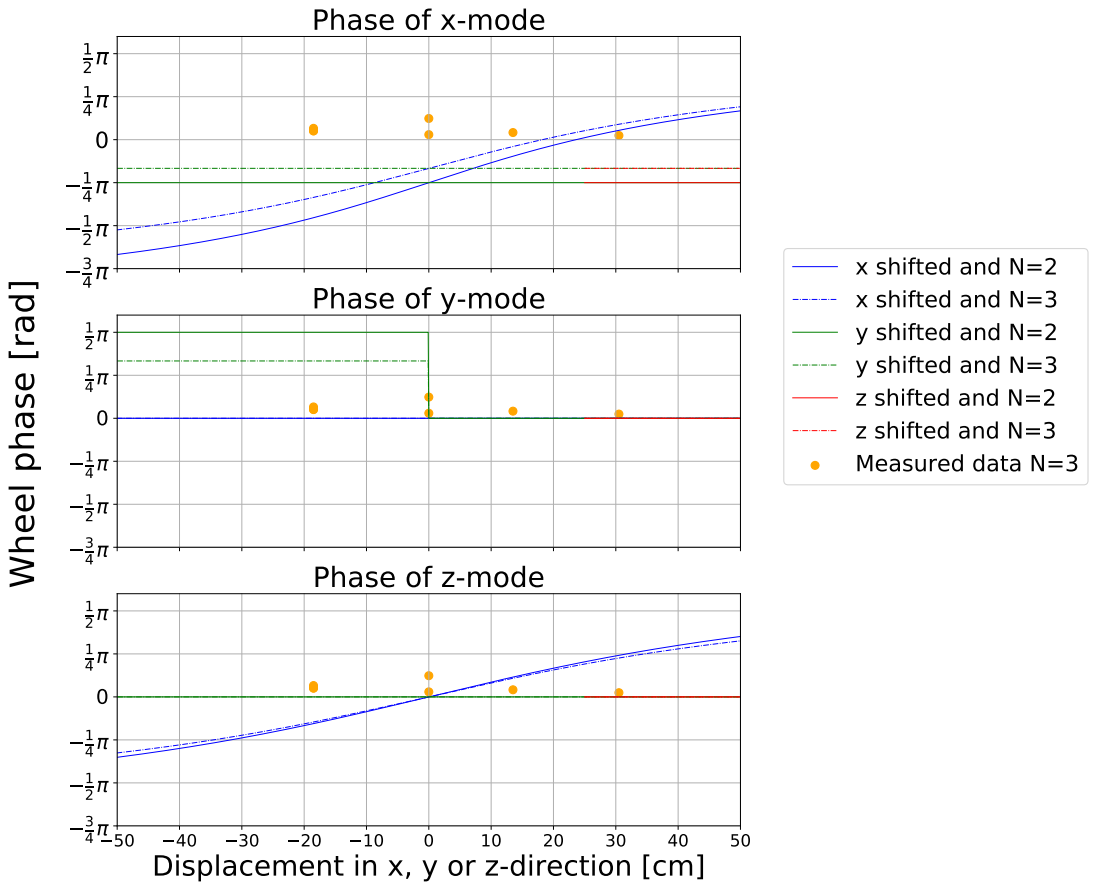

Figure 4.12: *The expected and measured phase of the gravitational force is plotted. The three graphs show the different modes, in x-, y-, and z-direction. The different colors show the different displacement directions. The solid lines show the expected values for a masswheel with two masses (N=2) attached and the dashed lines the expected values for a masswheel with three masses (N=3) attached. The measured data is shown in each of the lateral directions because it is unknown which mode corresponds to this frequency. The measured data used three masses on the wheel (N=3).*

Figure 4.12 shows both the expected and the measured phase of the gravitational interaction. The measured phase at different locations is shown in each of the three lateral directions, because it is unknown which mode this frequency corresponds to. Note that the wheel turns in the xz-plane. For this reason the expected phase for the x-mode and y-mode have a different behaviour.

Chapter 5

Discussion

In this chapter the different results are discussed. The Q factor is determined in three different ways, these are compared to each other. Next, the two measurements of the vibration isolation are compared and at last the measurement of gravitational interaction is discussed.

5.1 Q factor

The Q factor is determined in three different ways. The first uses a magnetic ringdown, this results in a Q factor of $Q = 960 \times 10^3$. The other two values are determined using a Lorentzian fit onto the obtained spectrum. These result in the values $Q = 929 \times 10^3$ and $Q = 530 \times 10^3$. The values are within a difference of a factor of two, the average value is 806×10^3.

During the experiment it was noticed that the damping time decreased and therefore the Q factor decreased, while nothing on the set-up was changed. The value for the eigenfrequency also changed during the experiment, on a time scale of weeks.

Since these values of the Q factor were not measured within the same week, the value using a magnetic ringdown roughly nine days before the other two measurements, this could explain the differences. In the past it has also been seen that the Q factor of a magnetic resonator has a higher Q factor when driven hard then when driven softly. This is attributed to the increase in temperature of surface spins when the magnet moves a lot. The idea is that the polarization decreases when temperature increases and that this lowers the damping.

5.2 Vibration Isolation

The vibration isolation was measured in two different ways. The first used a mechanical actuator to create vibrations in the frame of the cryostat. This resulted in a damping of

111 dB. The second method used the rotating masswheel as a source of vibrations, this resulted in a damping of 92 dB.

The measured damping using the masswheel was lower than using the actuator. The masswheel creates not only mechanical vibrations, but also the gravitational signal. Therefore the difference between these two measured damping values could be explained by gravitational interaction between the masswheel and the levitating magnet.

If this difference in damping is caused by gravitational interaction, the difference in damping should change if the masswheel is changed in position. The gravitational coupling is larger if the distance between the magnet and the masswheel is smaller, therefore the measured data is plotted on top of the simulated gravitational force.

The difference in attenuation may also be attributed that the different sources of vibrations make the cryostat vibrate in a different direction and that the different vibration directions couple 19 dB differently to the trap.

5.3 Gravitational Interaction

In method subsection 3.6.1 the expected gravitational interaction is simulated. This simulation is used to compare to the measured data points. The results are shown in figure 4.11 for the amplitude and figure 4.12 for the phase.

Comparing the measured points for the amplitude it is most likely that this mode is not a y-mode. The values of the measured points do compare roughly with the values expected for the x-mode. A few of the data points coincide with the values expected for the shift in the x- or y-direction. The measurement was performed using a masswheel with three masses attached. The shape of the measured points do roughly fit the shape for the expected amplitude for the z-mode with a x- or y-displacement, but the values are on average too low. This could be caused by a systematic error in the measurement.

The measured data points for the phase are roughly on a line just above zero phase shift. The wheel turns in the xz-plane and the displacement was in the x-direction during the measurements. Only the y-mode shows a flat behaviour for displacement in the x-direction.

However if the xz-plane of the wheel is not aligned with the xz-plane of the trap, the displacement of the wheel could also have a component in the y-direction of the trap. Rotation of the trap with respect to the wheel can occur, one of the reasons could be spring stiffening during the cool down, this effect is currently not measurable. If this is the case, the measured data also matches displacement in the y-direction for the x- and z-mode.

The calibration of the measured data could be off by a constant factor. For all possible matches with the simulation this would result in a constant shift, therefore in the phase explanations above the constant offset is not taken into account.

There always remains the option that the used frequency corresponds to a rotational mode instead of a translational mode. With the current measurements this can't be excluded.

Chapter 6

Conclusion & Outlook

In this thesis a method is explained and described to detect gravitational interaction between small particles in the order of milligrams and larger masses in the order of kilograms. When this method is extrapolated to a method to detect gravitational interaction between two masses in the order of milligrams, the regime between quantum mechanics and general relativity can be investigated.

This experiment uses a Meissner levitating micro particle having a mass of roughly 1.5 mg levitating inside a superconducting lead trap. The fact that the magnet levitates is shown by a magnetic ringdown, the magnet is driven magnetically and a ringdown is measured. This was performed at several frequencies. At a frequency of 52.505 Hz a Q factor of 960×10^3 is determined. Using the levitating magnet the mechanical damping in the system was measured in two different ways. The first measurement used a mechanical actuator to create vibrations in the frame of the cryostat and resulted in a damping of 111 dB. The second measurement used the rotating masswheel as a source of vibrations and resulted in a damping of 92 dB.

The difference in the damping could be caused by gravitational interaction between the magnet and the rotating masswheel. The amplitude of the gravitational interaction is of the correct order of magnitude for gravitational interaction between the levitating magnet and the rotating masses. The amplitude and phase of the gravitational interaction however do not agree with any of the three vibrational modes that would be sensitive to a gravitational interaction. The amplitude suggests it would be an x- or z-mode with an x- or y-displacement while the phase suggests it would be either the y-mode with an x-displacement or the x- or z-mode with a y-displacement.

There always remains the option that the used frequency corresponds to a rotational mode instead of a translational mode. With the current measurements this can't be excluded.

For future research the measurements could be repeated for the other frequencies to determine which frequency corresponds with which mode. A second pickup loop detected with a second SQUID could also provide the information to determine which mode is which, by looking at the phase differences between the two pickup loops.

More measurements on the DC value of the SQUID or the shift in resonance frequency could also provide a measurement on the gravitational interaction between the magnet and the moon or the magnet and the tides of the sea water.

A new version of this experiment could be designed where two lead traps are close to each other and the gravitational interaction between the two magnets could be detected. It is crucial that the magnetic fields of the particles are well shielded such that they don't have a magnetic interaction. The size and masses of the particles could be decreased to approach the regime between quantum mechanics and general relativity. One of the masses for example could be brought in superposition, while having gravitational interaction with the other mass.

In the set-up of the cryostat the vibration isolation could be optimised for frequencies below 100 Hz. Currently the vibration isolation is optimised for 1 kHz or higher. This would result in a better mechanical damping.

For experiments using the same principle of a masswheel the masswheel itself can also be optimised. Placing the masswheel inside a vacuum chamber would cause the acoustic vibrations to decrease a lot. The displacement of the wheel is currently done by hand, this could be automated and optimised. If the masswheel can slide across its bridge the measurements would be more accurate since the locations are more reproducible. The distance between the measured points would also be more precise and consistent.

All of the improvements could eventually lead to detecting gravitational interaction on smaller scales than ever before. This enables a new approach to investigate the regime in between quantum mechanics and general relativity.

Acknowledgments

Ik heb zo ontzettend genoten van dit master project, het heeft me allerlei nieuwe dingen geleerd en tot nieuwe inzichten gebracht over de collegestof van de afgelopen zes jaar. Dit leerzame proces was natuurlijk niet mogelijk geweest zonder de fantastische onderzoeksgroep waar ik in beland ben. Daarom bedank ik heel graag de gehele Oosterkamp-groep-familie, zonder de groep was dit allemaal niet mogelijk geweest en lang niet zo leerzaam geworden. In het bijzonder kijk ik dan naar Tjerk, Tim en Jaimy, de drie vaste groepsleden die er al vanaf het begin bij waren en met wie ik ontzettend veel plezier heb gehad en leerzame gesprekken mee heb gevoerd. Verder heb ik me altijd welkom gevoeld door de rest van de groep; Koen, Evert, Eli, Gesa en Bernard, bedankt voor jullie moeite en de gezelligheid die we altijd hebben gehad.

Tijdens dit project heb ik niet alleen dingen over natuurkunde zelf geleerd. Het heeft me ook laten inzien dat experimenten als deze totaal niet mogelijk zouden zijn zonder de hulp van technici. De FMD en de ELD hebben alle benodigde spullen geleverd en adviezen gegeven, ook als ze daar zelf even niet op zaten te wachten.

Het voelt raar om nu toch echt klaar te zijn met dit project. Ik hoop ontzettend dat mijn volgende project net zo leuk, leerzaam en gezellig zal verlopen als deze. Dan ben ik klaar om mijn diploma in ontvangst te nemen en om (helaas) een punt achter mijn studentenleven te zetten.

Scripsi.

References

[1] M. F. Gely and G. A. Steele, *Superconducting electro-mechanics to explore the effect of general relativity in massive superpositions*, (2021).

[2] T. Westphal, H. Hepach, J. Pfaff, and M. Aspelmeyer, *Measurement of Gravitational Coupling between Millimeter-Sized Masses*, (2020).

[3] A. Vinante, P. Falferi, G. Gasbarri, A. Setter, C. Timberlake, and H. Ulbricht, *Ultralow mechanical damping with Meissner-levitated ferromagnetic microparticles*, (2020).

[4] M. Physics, *Meissner effect. – The art of levitation*, 2020.

[5] R.F. Gasparovic and W.L. McLean, *Superconducting Penetration Depth of Lead*, Physical Review B - Condensed Matter and Materials Physics **2**, 2519 (1970).

[6] D. J. Griffiths, *Introduction to Electrodynamics*, Pearson, fourth edition, 2014.

[7] J. van Soest, *Meissner Levitated Magnetic Microparticle, MSc thesis*, 2020.

[8] Q. G. Lin, *Theoretical development of the image method for a general magnetic source in the presence of a superconducting sphere or a long superconducting cylinder*, Physical Review B - Condensed Matter and Materials Physics **74**, 1 (2006).

[9] G. Wijts, *Magnetic Resonance Force Microscopy at milliKelvin Temperatures*, PhD thesis, 2013.

[10] M. de Wit, *Advances in SQUID-detected Magnetic Resonance Force Microscopy*, PhD thesis, 2019.

[11] J. Cochran and D. Mapother, *Superconducting Transition in Aluminum*, Physical Review **111**, 132 (1958).